NASA CONTRACTOR REPORT

THEORETICAL EFFECT OF SEED OPACITY AND TURBULENCE ON TEMPERATURE DISTRIBUTIONS IN THE PROPELLANT REGION OF A VORTEX-STABILIZED GASEOUS NUCLEAR ROCKET

by R. B. Kinney

Prepared by
UNITED AIRCRAFT CORPORATION
East Hartford, Conn.
for

NATIONAL AERONAUTICS AND SPACE ADMINISTRATION • WASHINGTON, D. C. • MARCH 1967

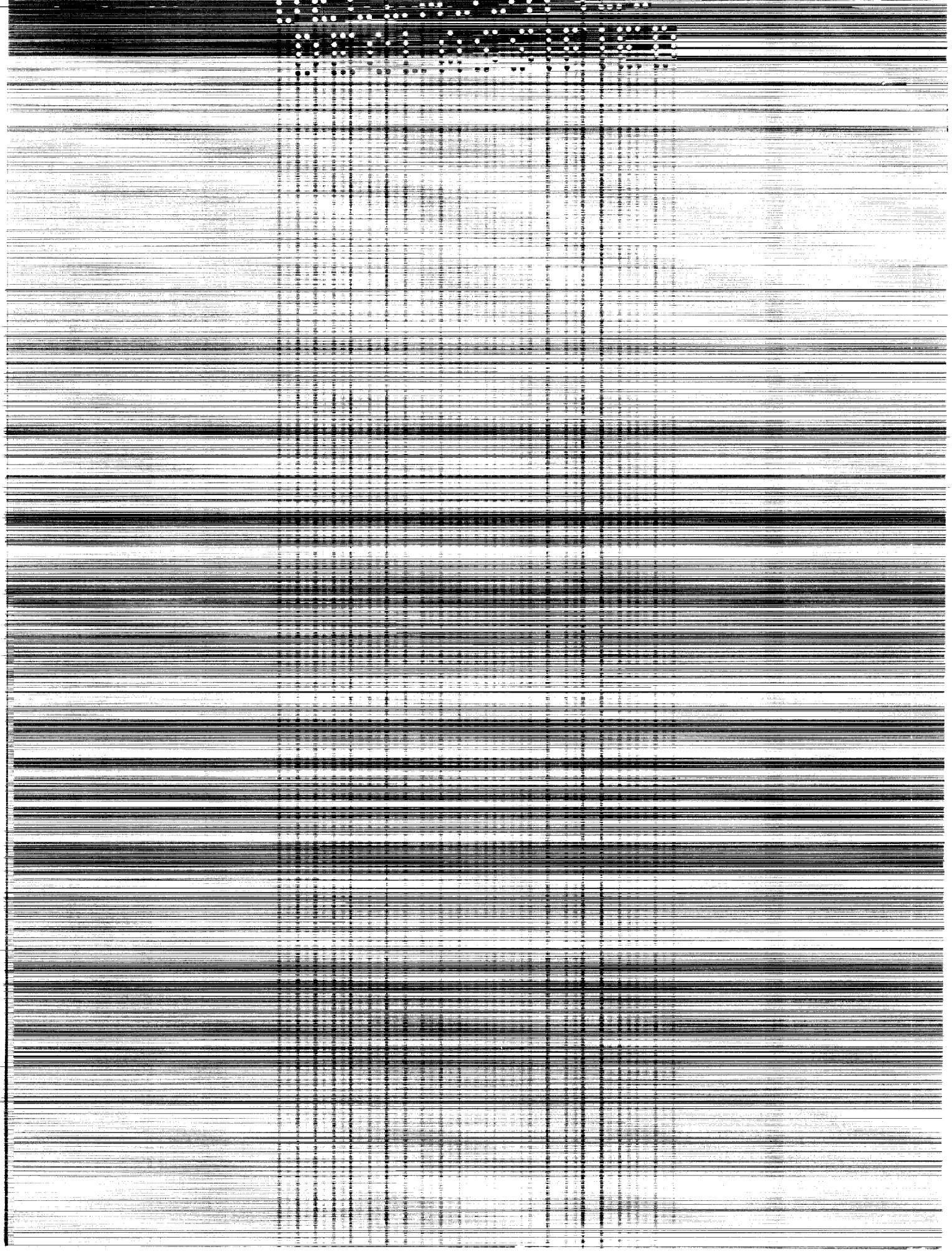

NASA CR-694

THEORETICAL EFFECT OF SEED OPACITY AND TURBULENCE ON TEMPERATURE DISTRIBUTIONS IN THE PROPELLANT REGION OF A VORTEX-STABILIZED GASEOUS NUCLEAR ROCKET

By R. B. Kinney

Prepared under Contract No. NASw-847 by
UNITED AIRCRAFT CORPORATION
East Hartford, Conn.

for

NATIONAL AERONAUTICS AND SPACE ADMINISTRATION

FOREWORD

An exploratory experimental and theoretical investigation of gaseous nuclear rocket technology is being conducted by the United Aircraft Corporation Research Laboratories under Contract NASw-847 with the joint AEC-NASA Space Nuclear Propulsion Office. The Technical Supervisor of the Contract for NASA is Captain W. A. Yingling (USAF). Results of the investigation conducted during the period between September 15, 1965 and September 15, 1966 are described in the following six reports (including the present report) which comprise the required fourth Interim Summary Technical Report under the Contract:

1. Krascella, N. L.: Theoretical Investigation of the Absorptive Properties of Small Particles and Heavy-Atom Gases. NASA CR-693, 1967. (Unclassified)

2. Kinney, R. B.: Theoretical Effect of Seed Opacity and Turbulence on Temperature Distributions in the Propellant Region of a Vortex-Stabilized Gaseous Nuclear Rocket (U). NASA CR-694, 1967. (report classified Confidential) (present report)

3. Kesten, A. S., and N. L. Krascella: Theoretical Investigation of Radiant Heat Transfer in the Fuel Region of a Gaseous Nuclear Rocket Engine. NASA CR-695, 1967. (Unclassified)

4. Roback, R.: Theoretical Performance of Rocket Engines Using Gaseous Hydrogen in the Ideal State at Stagnation Temperatures up to 20,000 R. NASA CR-696, 1967. (Unclassified)

5. Latham, T. S.: Nuclear Criticality Study of a Specific Vortex-Stabilized Gaseous Nuclear Rocket Engine (U). NASA CR-697, 1967. (report classified Confidential)

6. McLafferty, G. H., H. E. Bauer, and D. E. Sheldon: Preliminary Conceptual Design Study of a Specific Vortex-Stabilized Gaseous Nuclear Rocket Engine (U). NASA CR-698, 1967. (report classified Confidential)

[redacted]

Theoretical Effect of Seed Opacity and Turbulence on Temperature Distributions in the Propellant Region of a Vortex-Stabilized Gaseous Nuclear Rocket (U)

TABLE OF CONTENTS

[redacted]

[redacted]

Theoretical Effect of Seed Opacity and Turbulence on Temperature Distributions in the Propellant Region of a Vortex-Stabilized Gaseous Nuclear Rocket (U)

SUMMARY

A theoretical investigation was conducted to determine the effect on the temperature and radiant heat transfer distributions in the propellant region of a vortex-stabilized gaseous nuclear rocket which result from: the use of newly defined opacity characteristics of solid and vaporized tungsten seed; and the introduction of turbulence in the region adjacent to the peripheral wall. In determining the effect of turbulence level on the temperature distribution, values of turbulence level were used which bracket that which is expected in a specific vortex-stabilized gaseous nuclear rocket engine configuration under study at the Research Laboratories. The turbulence calculations include allowance for the stabilizing effect of radial temperature gradients and radial circulation gradients on the basis of hypotheses by G. I. Taylor and L. Prandtl concerning the effect of Richardson number on turbulence.

[redacted]

CONCLUSIONS

1. The effect of recently calculated changes in the opacity of solid and vaporized tungsten seed is to increase the required thickness of the low-temperature portion of the propellant region near the peripheral wall of a vortex-stabilized rocket engine. For a radial weight flow of 1.0 $lb/sec\text{-}ft^2$, the thickness of the region bounded by temperatures of 4000 and 20,000 R is increased by approximately 50 percent over that determined using previous opacity information.

2. The calculated thermal conductivity due to turbulence near the peripheral wall of a specific vortex-stabilized gaseous nuclear rocket engine being analyzed at the Research Laboratories is approximately equal to the radiation thermal conductivity for temperatures less than approximately 40,000 R.

3. Hypotheses by G. I. Taylor and L. Prandtl concerning the effect of Richardson number on turbulence indicate that radial temperature gradients and circulation gradients in a vortex-stabilized gaseous nuclear rocket engine will substantially reduce the turbulence created by viscous effects in the fluid near the peripheral wall of the engine as this fluid flows radially inward towards the fuel-containment region.

INTRODUCTION

The energy transfer to the propellant gas in a vortex-stabilized gaseous nuclear rocket is provided by thermal radiation emitted from the fuel-containment region. In order to insure that sufficient energy is absorbed by the propellant, it has been necessary to consider seeding the propellant to augment its low-temperature opacity. In this way, it is possible to achieve high propellant enthalpy levels as well as to effectively shield the rocket chamber walls from high-intensity thermal radiation.

In previous studies (Refs. 1, 2, 3, and 4) the thickness of the seeded propellant necessary to absorb the required amount of incident thermal radiation was determined for different opacity characteristics of the seed material. It was found that the absorbing distances and, equally as important, the magnitude and wave number distribution of the spectral heat flux were strongly dependent on the seed opacity characteristics. Therefore, a continuing effort has existed to define more accurately the absorption properties of the seed and to determine the subsequent changes in the radiant heat transfer characteristics of the system. Additionally, because the existence of turbulence in the peripheral-wall region of the vortex chamber may have a marked influence on the temperature distribution, thereby affecting the radiant heat transfer, it has become necessary to include the effects of turbulence in the heat transfer calculations.

The objective of the present work is to calculate temperature profiles and heat flux distributions for newly defined absorption characteristics of the solid and vaporized seed (tungsten). Results are to be obtained for cases where the effect of turbulence is excluded (in analogy with previous work done on this subject) and for cases where the effects of turbulence have been included.

ANALYTICAL MODEL OF PROPELLANT REGION

Physical Description and Assumptions

The analytical model employed to calculate temperature distributions in the propellant region is essentially the same as that of Ref. 4. The Flow pattern on which the analytical model is based is shown in Fig. 1.

The portion of the propellant region which is of interest in the present calculations is that near the peripheral wall where changes in propellant opacity characteristics plus turbulence effects have the greatest influence on the temperature distribution. For simplicity in analyzing this region, it has been assumed that the axial velocity in this region is zero (i.e., the analysis applies where x is less than x_2). The assumption of zero axial velocity leads to a constant radial hydrogen weight flow in the region bounded by the end walls of the vortex chamber. The assumptions which are required for the analysis are as follows:

1. The distance between the inner boundary of the region analyzed and the wall of the vortex tube is sufficiently small relative to the radius of the heat source that changes in circumference in this region can be neglected.

2. The temperature at a given radius is independent of axial distance. Except for end-wall boundary layer regions, this assumption is justified by the radial density stratification due to flow rotation (see Ref. 1). Changes in temperature with axial distance due to axial heat flux near the end wall are neglected.

3. The ratio of seed density to hydrogen density is constant and, therefore, opacity is independent of axial distance at a given radius. Also, from Assumption 2, the magnitude of the radial radiant heat transfer rate at a given radius is independent of axial distance, and the net radiant heat transfer in the axial direction is zero.

4. Heat transfer by molecular thermal conduction is negligible relative to heat transfer by thermal radiation and heat transfer due to turbulence.

5. The heat transfer is steady with respect to time.

6. The peripheral wall of the vortex chamber absorbs all incident thermal radiation and emits as a black body at the wall temperature of 4000 R.

Analysis

In this analysis, the simultaneous transport of heat by thermal radiation, convection, and turbulence is considered. On the basis of the foregoing assumptions, the heat transferred by these three modes across an arbitrary plane in the propellant region is independent of both radius and axial distance. This condition can be written

$$Q_{conv} + Q_{rad} + Q_{turb} = \text{const} \tag{1}$$

which is equivalent to the following differential form

$$\frac{d}{dr}(Q_{conv}) + \frac{d}{dr}(Q_{rad}) + \frac{d}{dr}(Q_{turb}) = 0 \tag{2}$$

The radial derivatives of the heat flux quantities can now be related to the temperature gradient by the following expressions

$$\frac{d}{dr}(Q_{conv}) = -W_R C_P \frac{dT}{dr} \tag{3}$$

$$\frac{d}{dr}(Q_{turb}) = -\frac{d}{dr}\left(\rho \epsilon_a C_P \frac{dT}{dr}\right) \tag{4}$$

where ϵ_a is the turbulent heat diffusivity (see Ref. 5). The radial derivative of the radiative heat flux is slightly more complicated to express and will be introduced at a later point in the development. In terms of the above quantities, the heat balance equation is

$$-W_R C_P \frac{dT}{dr} = -\frac{d}{dr}(Q_{rad}) + \frac{d}{dr}\left(\rho \epsilon_a C_P \frac{dT}{dr}\right) \tag{5}$$

It is required to determine the temperature distribution which will satisfy Eq. (5).

In previous calculations (Refs. 1 to 4), the effect of turbulence on the heat transfer was not considered; that is, ϵ_a was equal to zero. In the present investigation, calculations are made for zero and nonzero values of ϵ_a. Because the analytical development is somewhat different depending on whether or not turbulence effects are included, it is expedient to treat these two situations separately.

Effects of Turbulence Excluded

Under these conditions, the analysis is identical to that given in Ref. 4 and need not be given in detail here. Only the important results will be summarized.

The propellant region is divided into two discrete zones, one zone being considered as optically thick to thermal radiation and the other being considered as optically thin to radiation.

In the optically thick zone the gradient of the radiant heat flux is given by the Rosseland approximation

$$\frac{d}{dr}\,(Q_{rad}) = -\frac{16\sigma}{3}\,\frac{d}{dr}\left(\frac{T^3}{a_R}\,\frac{dT}{dr}\right) \tag{6}$$

where a_R is the Rosseland mean opacity of the propellant and is given by

$$a_R = \frac{\int_0^\infty \frac{\partial B_\omega}{\partial T}\,d\omega}{\int_0^\infty \frac{1}{a_\omega^*}\left(\frac{\partial B_\omega}{\partial T}\right)d\omega} \tag{7}$$

and a_ω^* is the spectral absorption coefficient of the propellant adjusted for stimulated emission. This quantitiy is related to the spectral absorption coefficient by

$$a_\omega^* = a_\omega\left[1 - e^{-hc\omega/kT}\right] \tag{8}$$

In the optically thin zone the gradient of the radiant heat flux is given by (see Ref. 4)

$$\frac{d}{dr}\,(Q_{rad}) = -\left[n_R'\,\bar{a}\,Q_{rad} - 4\,a_p\sigma T^4\right] \tag{9}$$

where n_R' is the modified radiation attenuation parameter and $\bar{a}$ is the flux mean opacity given by

$$\bar{a} = \frac{\int_0^\infty a_\omega^* Q_\omega d\omega}{\int_0^\infty Q_\omega d\omega} \tag{10}$$

The modified radiation attenuation parameter has the value $n_R' = 2$ if it is assumed that (1) the radiation emitted by the optically thick region can be represented by a black body radiating at some characteristic temperature, and (2) the radiation directed backward from the peripheral wall region is negligible compared to the radiation directed from the high-temperature region. In performing the actual calculations, it has been found to be expedient to replace $n_R'/\bar{a}$ by $n_R a_R$ in Eq. (1) and to make the approximation $a_P \cong a_R$.

On the basis of the foregoing considerations, the heat balance equations which must be solved in order to obtain the temperature distribution are

$$-W_R C_P \frac{dT}{dr} = \frac{16\sigma}{3} \frac{d}{dr} \left(\frac{T^3}{a_R} \frac{dT}{dr} \right) \tag{11}$$

in the optically thick zone, and

$$-W_R C_P \frac{dT}{dr} = (n_R Q_{rad} - 4\sigma T^4) a_R \tag{12}$$

in the optically thin zone.

Effects of Turbulence Included

Peripheral-wall turbulence has the effect of reducing temperature gradients in the propellant region. Thus a greater distance is required to produce a given change in temperature when turbulence is present than when the flow is laminar. An increase in the thickness of the propellant region will result in the desirability of using diffusion analysis rather than transport analysis to compute the radiant heat transfer. In addition, the use of transport analysis for calculating radiant heat transfer and diffusion analysis for calculating heat transfer by turbulence would result in severe mathematical difficulties. Therefore, all of the calculations described in the following paragraphs have been carried out using diffusion analysis in analyzing both radiative and turbulent heat transfer. Under

these conditions the heat balance equation becomes (see Eq. (5)).

$$- W_R C_P \frac{dT}{dr} = \frac{16\sigma}{3} \frac{d}{dr}\left(\frac{T^3}{a_R} \frac{dT}{dr}\right) + \frac{d}{dr}\left(\rho \epsilon_a C_P \frac{dT}{dr}\right) \tag{13}$$

Representation of the radiative and turbulent heat transfer as purely diffusive in nature leads to the introduction of an effective thermal conductivity which includes the radiant and turbulent transport of heat, but neglects that due to molecular motion. Such an effective thermal conductivity can be written.

$$K_e = K_r + K_t = \frac{16\sigma T^3}{3a_R} + \rho \epsilon_a C_P \tag{14}$$

In terms of this quantity the heat balance equation becomes

$$- W_R C_P \frac{dT}{dr} = \frac{d}{dr}\left(K_e \frac{dT}{dr}\right) \tag{15}$$

In the foregoing expression for K_e, the quantities ρ, C_P, and a_R are well-defined functions of temperature once the composition and opacity characteristics of the propellant are specified. ϵ_a is a function of the turbulent motion and will be discussed further in a later section.

CALCULATION PROCEDURES

The analytical procedures which have been employed for determining the temperature and heat flux distributions within the propellant region of the vortex-stabilized gaseous nuclear rocket are currently formulated in two programs: a main computer program which treats "spectral" thermal radiation and a separate program which treats "gray gas" thermal radiation. In both programs "diffusion" or "transport" analysis is used depending on whether the medium is optically "thick" or "thin," respectively.

Main Computer Program

The main computer program (see Ref. 6) permits calculation of spectral heat flux for a specified temperature distribution. In the machine computations, a choice can be made at each station and each wave number to determine whether a transport or diffusion analysis will result in a better approximation to the actual flux. Transport analysis was used in the majority of the spectral heat flux calculations. In the present report, spectral heat flux was calculated at the following wave numbers: 1000, 2500, 4000, 6000, 8000, 10,000, 12,000, 15,000, 18,000, 21,000, 24,000, 27,000, 30,000, 33,000, 36,000, 39,000, 42,000, 50,000, 58,000, 66,000, 74,000, 82,000, 90,000, 100,000, 110,000, 125,000, and 140,000 cm^{-1}. The total heat flux is determined by integrating the spectral heat flux over all wave numbers. This main computer program cannot be used for problems where the temperature distribution cannot be specified.

Simplified Computer Program

The simplified computer program permits calculation of the temperature distribution by employing a gray-gas analysis of the propellant region. As outlined in the description of the analytical model, the entire region is divided into optically thick and optically thin zones (when turbulence effects are considered, the optically thick zone comprises the entire propellant region). In the optically thick region, the temperature distribution can be calculated directly by integrating Eqs. (11) and (13) for a specified (constant) radial weight flow, W_R , the known physical properties of the propellant, and a law for the variation of ϵ_a with position. The calculation in the region where the gas can be considered optically thin is somewhat more complicated. In this region, an iterative procedure employing both the main and simplified computer programs must be used in order to obtain the temperature distribution.

In the iterative procedure, successive approximations to the temperature distribution are made until the energy balance condition is satisfied. This procedure

is followed only when turbulence effects are excluded. Under this condition, the energy balance equation which must be satisfied is (see Eq. (11)):

$$Q_{conv} + Q_{rad} = const = (Q_{conv} + Q_{rad})_w \tag{16}$$

where the constant has been evaluated using the known conditions existing at the peripheral wall. Making the approximation that $(Q_{rad})_w \cong 0$, Eq. (16) can be written

$$Q_{rad}(x) = Q_{conv} - (Q_{conv})_\omega = W_R \int_{T_w}^{T(x)} C_p dT \tag{17}$$

It must be kept in mind that Eq. (17) is not an expression for Q_{rad}. This quantity is calculated separately by the main computer program for a specified temperature distribution and specified absorption characteristics of the propellant.

The procedure is to assume initial values for the variation of n_R with temperature and to calculate the corresponding temperature distribution using Eqs. (12) and (17). The temperature distribution is then introduced into the main computer program and the radiant heat flux, Q_{rad}, is calculated. A new distribution of n_R with temperature is then calculated on the basis of the heat flux determined from the main computer program using the relation

$$n_R = \frac{1}{Q_{rad}} \left[4\sigma T^4 - \frac{1}{a_R} \frac{d}{dr} (Q_{rad}) \right] \tag{18}$$

Using the calculated variation of n_R with temperature, the iterative procedure is repeated until Eq. (17) is satisfied.

PROPELLANT OPACITY CHARACTERISTICS

The propellant is composed of hydrogen which has been seeded with solid tungsten particles prior to injection at the peripheral wall. At any radial station in the flow, therefore, the opacity of the propellant is the sum of that due to the hydrogen plus that due to the tungsten. In the present investigation, the tungsten contributes to the propellant opacity either in the solid or vapor phase (a liquid phase is not considered) according to whether the propellant temperature is above or below the tungsten vaporization temperature (taken to be 11,000 R at a pressure of 1000 atm). The opacity, expressed in terms of the spectral absorption coefficient, in general depends on the frequency of thermal radiation as well as the temperature.

The spectral absorption coefficients of hydrogen used in the present calculations are identical to those used in a previous report (Ref. 4). In arriving at these absorption coefficients, the absorption due to the Lyman- α line has been neglected. It is felt that neglecting this opacity contribution provides a more realistic model on which to base radiant heat transfer calculations.

The spectral absorption coefficients for the solid and vaporized seed used in the present calculations are shown as the solid curves in Figs. 2 and 3, respectively. For purposes of comparison, the absorption coefficients used in previous calculations (Ref. 4) are shown as the dashed curves. The new opacity curves are based on information contained in Ref. 7.

The principal change in the absorption coefficient for the solid seed has resulted from an increase (from 0.2 to 2) in the total oscillator strength of the seed in order that this oscillator strength agree with the value used in calculating the opacity of the vaporized tungsten. This increase in oscillator strength has resulted in an extension of high values of the spectral absorption coefficient well into the ultraviolet region (high-wave-number region). Additionally, the spectral absorption coefficient has been modified slightly in the low-wave-number range as well. The new values in the low-wave-number range were obtained from an analytical extrapolation of recent index of refraction data gathered in the visible and infrared regions. For further discussion of these opacity changes, the reader is referred to Ref. 7.

The spectral absorption coefficient for the vaporized tungsten has been modified in order to take into account a new, and probably more accurate, oscillator strength distribution with wave number (the total oscillator strength remains unchanged) in the bound-bound (or line) region of the spectrun.

The total spectral absorption coefficients of the propellant (hydrogen plus tungsten) are shown in Fig. 4. In arriving at these curves, the density of the tungsten seed was assumed to be 3 percent of that of hydrogen for both solid and

vapor phases. For temperatures greater than 19,000 R, the propellant opacity is primarily due to absorption by the hydrogen at all wave numbers. A comparison of the propellant spectral absorption coefficients used in the present calculations and those of a previous report (Ref. 4) is presented in Fig. 5.

Although spectral absorption coefficient information is required for exact determination of the radiant heat flux in an absorbing and emitting gas, significant results can be obtained in some instances by employing a gray-gas analysis based on an average value of opacity. One such average is the Rosseland mean opacity as given in Eq. (7). The Rosseland mean opacity of the propellant mixture calculated using spectral absorption coefficient information such as that given in Fig. 4 is shown in Fig. 6. For purposes of comparison, the values used in previous calculations are also shown in Fig. 6. The most pronounced change in Rosseland mean opacity occurs in the temperature range between 10,000 R and 15,000 R where the opacity characteristics of the vaporized tungsten have the strongest influence. At temperatures above 20,000 R the propellant opacity is essentially that of hydrogen which has remained unchanged.

It is of interest to compare the variation with temperature of the Rosseland mean opacity and spectral absorption coefficients. Such a comparison is made in Fig. 7 for three different wave numbers.

RESULTS AND DISCUSSION

Effects of Turbulence Excluded

The variation of the total heat flux with temperature in the propellant region is shown in Fig. 8. For a given constant radial weight flow of propellant, the heat flux variation with temperature is only a function of the thermodynamic state of the gas and, therefore, is universal for all results to be presented in this section. As can be seen from the figure, the heat fluxes are assumed to approach zero at the wall temperature of 4000 R. This is a necessary requirement imposed on the simplified computer program; the heat flux at the propellant temperature of 60,000 R is adjusted until this requirement is satisfied.

In the present calculations, three values for the propellant radial weight flow were chosen. Figures 9 and 10 illustrate, respectively, the influence of the radial weight flow on the radiation attenuation parameter, n_R, and the corresponding temperature distributions. The results from a previous report (Ref. 4) are also shown for comparison. The curves shown in Figs. 9 and 10 are the final results obtained after successive iterations between the main and simplified computer programs. As discussed in the analysis section, this iterative procedure is required only when the propellant is optically thin to thermal radiation. Therefore, curves for n_R were calculated only in the low-temperature region adjacent to the peripheral wall. This region begins at approximately 22,000 R for the chosen radial weight flows of 1.0 and 0.5 lb/sec-ft^2. As the radial weight flow decreases, the temperature at which the region becomes optically thin decreases correspondingly. In fact, for a radial weight flow of 0.1 lb/sec-ft^2 the region is sufficiently thick to thermal radiation that the iterative procedure cannot be applied and diffusion analysis was used throughout. This explains the absence of a calculated n_R distribution in Fig. 9 for this case.

Referring to Fig. 10, it is seen that the temperature distribution for W_R = 1.0 lb/sec-ft^2 is changed very little compared to that obtained using previous opacity information. Also the effect of decreasing the radial weight flow is to increase the thickness of the propellant region, in agreement with the results of Ref. 4.

The spectral heat flux distributions with wave number corresponding to the three radial weight flows investigated are shown in Figs. 11, 12, and 13 for several representative temperatures. These curves serve to illustrate the indirect effect of radial weight flow on the spectral heat flux distributions through direct changes in absorbing distances.

It can be seen that the curves in each of Figs. 11, 12, and 13 exhibit a characteristic dip in the wave number range between 20,000 and 50,000 cm^{-1}, and that this dip becomes more pronounced as the radial weight flow decreases. Referring to

Fig. 4, it is seen that this is also the wave number range in which the spectral absorption coefficient of the propellant exhibits large peaks. Thus as the radial weight flow decreases, thereby increasing the absorbing distances, more energy in this wave number range is absorbed by the intervening propellant layers. When the propellant is very thick, as is the case when $W_R = 0.1$ lb/sec-ft^2, no energy emitted from the high-temperature region (characterized by large wave numbers) is able to penetrate the low-temperature propellant layers adjacent to the peripheral wall.

The total heat flux at any temperature is obtained from an integration of the spectral heat flux, Q_ω, over all wave numbers. This integration is performed by the main computer program at each of twenty-one specified temperatures. The total heat flux obtained in this way is given in Figs. 14, 15, and 16 for each of the three temperature distributions shown as the solid curves in Fig. 10.

In Figs. 14 through 16, the symbols represent the calculated points obtained from the main computer program. These values correspond to the quantity Q_{rad} given as the left hand side of Eq. (17). The solid curve represents the results obtained from the simplified computer program and corresponds to the right side of Eq. (17). The close agreement between these two independently calculated quantities indicate that the energy balance condition has been satisfied.

An interesting point arises in connection with Fig. 16. As mentioned earlier, the diffusion approximation to thermal radiation was used in the entire propellant region by the simplified program in order to obtain the temperature distribution shown in Fig. 10 for $W_R = 0.1$ lb/sec-ft^2. This resultant temperature distribution was then used in the main computer program in order to calculate Q_{rad}. In this program, transport analysis was used throughout. Therefore, not only does Fig. 16 indicate that the energy balance condition was closely satisfied, it also illustrates that the total radiative heat flux as given by transport analysis does, in fact, converge to the diffusion approximation as the medium becomes optically thick.

Discussion of the Radiation Attenuation Parameter

The radiation attenuation parameter, n_R (see Fig. 9), accounts for many complicated characteristics of the actual radiation process. Its major influence on the analysis is two fold. First, it provides a convenient means for correcting the Rosseland mean opacity to correspond more closely to the effective opacity of the gas. Second, it accounts for the fact that the radiation streaming through the gas travels in all directions. However, the fact that those two major influences occur simultaneously complicates a more general quantitative interpretation of n_R. Nevertheless, it is possible to separate these two influences in an approximate fashion.

This is accomplished by introducing the modified radiation attenuation parameter, n_R', already defined and repeated here,

$$n_R' = \frac{n_R a_R}{\bar{a}} \tag{19}$$

The term $\bar{a}$ has already been given in Eq. (10) as

$$\bar{a} = \frac{\int_0^\infty a_\omega^* Q_\omega d\omega}{\int_0^\infty Q_\omega d\omega}$$

Using the spectral opacity and heat flux results obtained for each of the temperature distributions, the flux mean opacity of the gas, $\bar{a}$, was calculated. A comparison between $\bar{a}$ and the Rosseland mean opacity, a_R, is given in Fig. 17 for the three propellant radial weight flows of 1.0, 0.5, and 0.1 lb/sec-ft^2 and a pressure of 1000 atm.

As mentioned earlier in the analysis section, if the radiative transport in the optically thin region is described by the optically thin approximation, $\bar{a}$ is the effective opacity of the propellant and $n_R' = 2$ at all temperatures. Therefore, the degree to which the medium can be considered as optically thin to radiation can be inferred from values of n_R' calculated from Eq. (19). These values have been calculated for representative temperatures, and the results are shown in Fig. 18. The optically thin approximation ($n_R' = 2$) is also shown as the horizontal line. It can be seen that the optically thin approximation is a reasonably good average representation of the calculated values of n_R'.

Effects of Turbulence Included

The turbulent transport of heat is represented in the usual manner in the following calculations as a diffusive process. In analogy with the diffusion of heat by molecular means, a turbulent heat diffusivity coefficient, ϵ_a, is introduced. In contrast to molecular heat diffusion, however, ϵ_a is not a property of the fluid but is determined solely by the nature and structure of the turbulent fluid motion. The magnitude of this quantity must therefore be determined from fluid mechanical considerations.

Model for Turbulent Heat Diffusivity

In many turbulent flows, the turbulent transport of heat and momentum is due to the same mixing mechanism. For this reason, the exchange coefficient which characterizes the turbulent transport of momentum (the turbulent kinematic viscosity, ϵ_ν) bears a close relationship to ϵ_a. Therefore, a knowledge of ϵ_ν is usually all that is required in order that an estimate for ϵ_a can be made.

In the vortex chamber, the character of the turbulence at the peripheral wall is determined by a number of factors, the major one of which appears to be the jet mixing due to injection of the propellant. In order to calculate a value of ϵ_ν due to this factor, the relationship for a circular jet discharging into a quiescent fluid will be used. From Ref. 9, ϵ_ν is given by

$$\epsilon_\nu = 0.0256\ bU \tag{20}$$

where b is one quarter of the jet diameter and U is the velocity along the centerline of the jet. The variation of b and U with distance downstream of the jet is such that bU = constant (see page 596 of Ref. 9). Therefore, ϵ_ν is everywhere a constant in the region of jet mixing. To evaluate this constant, the conditions at the orifice of the jet will be used. Thus

$$\epsilon_\nu = 0.0256\ \frac{d_j}{4}\ V_j \tag{21}$$

where the approximation $V_j \cong U$ has been used. If the diameter of the jet is expressed in inches, the velocity is expressed in ft/sec, and ϵ_ν is expressed in ft^2/sec, the expression for ϵ_ν becomes

$$\epsilon_\nu = 0.000533 d_j\ V_j \tag{22}$$

Once the jet diameter and injection velocity are specified, values of ϵ_ν can be calculated.

Equation (22) is plotted in Fig. 19 as a function of the jet diameter for parametric values of the injection velocity. For the specific vortex-stabilized engine configuration considered in Ref. 10, the design values of injection jet diameter and injection velocity are 0.090 in. and 2400 ft/sec, respectively. Substitution of these values into Eq. (22) (see also Fig. 19) leads to an indicated value of ϵ_ν of 0.115 ft^2/sec.

Calculations were also made to determine the turbulence level associated with the boundary layer on the peripheral wall of the vortex chamber. These calculations were made for a velocity outside the boundary layer of 1370 ft/sec (reduced from the injection velocity by wall friction) and for an assumed wall boundary layer thickness of 0.25 in. The resulting average value of turbulent kinematic viscosity was 0.01 ft^2/sec and was calculated for an equivalent boundary layer on a flat plate. Although the boundary layer on a curved wall would probably be more turbulent than

one on a flat plate because of Taylor-Goertler instabilities, the resulting turbulence level is probably substantially less than that due to the injection jet. Therefore, within the accuracy of these calculations of turbulence levels, the total turbulence can probably be approximated as being equal to that due to the injection jet, as shown in Fig. 19.

Discussion of Turbulence Properties

A measure of the degree of turbulence can be obtained from a ratio of the turbulent and molecular kinematic viscosities, ϵ_ν/ν, where $\nu = \mu/\rho$. This ratio is shown in Fig. 20 for parametric values of ϵ_ν. In preparing this figure, values for ρ were obtained from Ref. 11, and values for μ were obtained from Refs. 12 and 13. It can be seen from Fig. 20 that, for fixed values of ϵ_ν, the turbulent transport of momentum relative to the molecular transport is greatest at the lowest temperatures. It should be noted that these curves also represent values of ϵ_α/α if it is assumed that the molecular and turbulent Prandtl numbers are unity (i.e., $\epsilon_\nu = \epsilon_\alpha$ and $\nu = \alpha$).

A convenient way of determining the relative magnitude of the transport of heat by turbulence and radiation can be obtained from an examination of the radiation and turbulent thermal conductivities expressed by Eq. (14). These quantities are shown in Fig. 21. The physical properties used in preparing these curves are shown in Fig. 22, and were obtained from Ref. 11.

The radiation thermal conductivity is shown as the single curve near the lower portion of Fig. 21. The turbulent thermal conductivity is plotted for parametric values of ϵ_α. It can be seen that, at sufficiently high temperatures, the radiation conductivity is predominant, even for turbulence levels an order of magnitude larger than those anticipated in the rocket design. As the temperature decreases, the turbulent heat transport represents a larger proportion of the total heat flow. For values of ϵ_α greater than approximately 0.5 ft^2/sec, heat is transported primarily by turbulence at temperatures below 45,000 R.

Effect of Flow Rotation on Turbulence

In the vortex chamber, flow rotation is present in a direction parallel to the peripheral wall in addition to the radial weight flow perpendicular to it. However, this tangential flow does not explicitly enter into the heat transfer analysis because there are no circumferential temperature or composition variations due to the flow stratification. Nevertheless, the presence of flow rotation does have a strong influence on the turbulent motion, and therefore, it does enter implicitly into the heat transfer through its effect on ϵ_α.

In the following analysis it is assumed that the stabilizing effect of flow rotation can be incorporated into the heat transfer analysis through the introduction

of a generalized Richardson number in analogy with the treatment of stratified turbulent flows in natural gravity fields. In rotating flows, however, the gravity effect must be replaced by that due to centrifugal acceleration. The generalized Richardson number is proportional to the ratio of the energy required to produce a radial displacement of a fluid particle against centrifugal forces to the energy imparted to the mean flow by turbulent shear work. This dimensionless parameter has been derived in Ref. 1 for the case where the shear force is caused by radial variations of the axial component of the flow. This result can be written

$$Ri = \frac{\frac{V_\phi^2}{r^2}\left(\frac{r}{\rho}\frac{d\rho}{dr} + \frac{2r}{\Gamma}\frac{d\Gamma}{dr}\right)}{\left(\frac{dV_z}{dr}\right)^2} \tag{23}$$

where V_ϕ and V_z are the tangential and axial components of the velocity, respectively, and Γ is the flow circulation given by $r V_\phi$.

In the present calculations, the axial component of velocity is zero. Thus the shear work is due to tangentially directed shear forces, and it is assumed that it is possible to replace dV_z/dr in Eq. (23) by $d V_\phi/dr - V_\phi / r$. Thus for the present purposes the generalized Richardson number is assumed to become

$$Ri = \frac{\frac{V_\phi^2}{r^2}\left(\frac{r}{\rho}\frac{d\rho}{dr} + \frac{2r}{\Gamma}\frac{d\Gamma}{dr}\right)}{\left(\frac{d}{dr}V_\phi - \frac{V_\phi}{r}\right)^2} \tag{24}$$

For practical calculations, it is convenient to write Eq. (24) in a modified form. Because the density variation of the propellant is primarily due to temperature changes, and if the state equation of the gas can be approximated by the ideal gas law (i.e., neglecting favorable density gradients due to dissociation and ionization of hydrogen), the density gradient term can be written

$$\frac{r}{\rho}\frac{d\rho}{dr} = -\frac{r}{T}\frac{dT}{dr} \tag{25}$$

Furthermore, approximating the circulation profile by the expression

$$\frac{\Gamma}{\Gamma_o} = \left(\frac{r}{r_o}\right)^{N_\Gamma} \tag{26}$$

the circulation gradient becomes

$$\frac{r}{\Gamma}\frac{d\Gamma}{dr} = N_\Gamma \tag{27}$$

and

$$\frac{dV_\phi}{dr} - \frac{V_\phi}{r} = \frac{V_\phi^2}{r^2}(N_\Gamma - 2)^2 \tag{28}$$

In terms of these quantities, the generalized Richardson number can be written

$$Ri = \frac{-\frac{r}{T}\frac{dT}{dr} + 2N_\Gamma}{(N_\Gamma - 2)^2} \tag{29}$$

Although little experimental information on the effect of Richardson number on turbulence is available, the limit of stability which has been proposed by G. I. Taylor (Ref. 14) for parallel flow in natural gravity fields is $Ri = 1$. In the present investigation, this criterion has also been adopted for the stability limit in rotating flows. Thus for values of the Richardson number less than unity, turbulence is assumed to exist. At Richardson numbers equal to or greater than unity, the flow is assumed to be completely laminar.

The effect of the dimensionless temperature gradient and the exponent in the circulation profile law, N_Γ, on the Richardson number is depicted in Fig. 23. For isothermal flow (corresponding to $M = 0$ in Fig. 23) it can be seen that the Richardson number increases for values of N_Γ greater than zero. At a value of $N_\Gamma = 0.76$, it is observed that $Ri = 1$ and the flow is assumed to be laminar. For positive values of M (as is the case near the peripheral wall) it can be seen that the flow is laminarized at still smaller values of N_Γ. For $M = 4$, the flow is stable for all positive values of N_Γ.

In incorporating the Richardson number effect into the heat transfer calculations, a functional relationship between ϵ_a and Ri is required. One possibility is to assume that ϵ_a is unaffected by Richardson number until $Ri = 1$, at which point ϵ_a is set equal to zero. A more realistic representation, however, should allow for the decrement of ϵ_a with increasing Richardson number in a continuous manner until $Ri = 1$, at which point ϵ_a is set equal to zero. Following this reasoning, Prandtl (Ref. 15) has recommended as a plausible relationship between ϵ_a and Ri the following expression

$$\epsilon_a = \epsilon_{a_0}(1 - Ri)^{1/2} \tag{30}$$

where ϵ_{a_0} is the value which would exist for Ri = 0. This relationship has been adopted here and is plotted in Fig. 24 for parametric values of ϵ_{a_0}. For values of Ri greater than unity, ϵ_a is identically zero.

Results of Heat Transfer Calculations

Temperature profiles have been calculated for a single radial weight flow of 1.0 lb/sec-ft^2 using a step-by-step procedure beginning at the peripheral wall of the vortex chamber. The radius of the vortex chamber was taken to be 100 cm (slightly greater than the radius of 3 ft = 91.5 cm for the engine of Ref. 10). At each step, the Richardson number is calculated from Eq. (29) using the local temperature gradient and specified (constant) value of N_Γ. Using this value for the Richardson number, a value of ϵ_a is calculated using Eq. (30) and a specified (constant) value for ϵ_{a_0}. The temperature contour is then obtained from an integration of Eq. (15).

Temperature profiles calculated using the above procedure are given in Fig. 25 for different turbulence levels represented by prescribed values of ϵ_{a_0}. The curves were calculated for $N_\Gamma = 0$, that is, for the case where the circulation profile has no effect on the laminarization of the flow. Nevertheless, without even this stabilizing influence, the temperature gradient does become sufficiently great to stabilize the flow. The location at which the flow becomes laminar due to the Richardson number exceeding unity is denoted by the vertical arrows on each curve. After laminarization occurs, the temperature curves rise steeply.

If the circulation profile is such that it contributes to the stability of the flow, the transition from turbulent to laminar flow occurs at locations closer to the peripheral wall. Denoting the width of the turbulent zone as the distance from the wall at which the Richardson number exceeds unity, it is possible to determine the extent of the turbulence as a function of N_Γ. These results are summarized in Fig. 26. It can be seen that even for $\epsilon_{a_0} = 0.6$ ft^2/sec, which is approximately six times the value envisioned in the full-scale engine design, the width of the turbulence zone is reduced drastically for increasing values of N_Γ. For N_Γ equal to or greater than 0.76, the turbulence disappears entirely. This point illustrates the importance of tailoring the tangential velocity profile such that the extent of the turbulence can be kept to a minimum. It should be noted, however, that no experimental evidence is available to verify the assumptions made concerning the effect of temperature gradient and circulation profiles on turbulence; as a consequence, the results shown in Figs. 25 and 26 should be considered more qualitative than quantitative at the present time.

REFERENCES

1. McLafferty, G. H.: Summary of Investigations of a Vortex-Stabilized Gaseous Nuclear Rocket Concept (U). Report RTD-TDR-63-1097, prepared by UAC Research Laboratories, November 1963. Confidential.

2. Saunders, A. R.: Theoretical Investigation of Radiant Heat Transfer in a Vortex-Stabilized Gaseous Nuclear Rocket (U). Report RTD-TDR-63-1096, prepared by UAC Research Laboratories. November 1963. Confidential.

3. McLafferty, G. H., and W. G. Burwell: Theoretical Investigation of the Temperature Distribution in the Propellant Region of a Vortex-Stabilized Gaseous Nuclear Rocket (U). UAC Research Laboratories Report C-910093-10, September 1964. Confidential. (Also issued as NASA CR-279.)

4. Kesten, A. S., and R. B. Kinney: Theoretical Effect of Changes in Constituent Opacities in Radiant Heat Transfer in a Vortex-Stabilized Gaseous Nuclear Rocket (U). UAC Research Laboratories Report D-910092-5, September 1965. Confidential.

5. Eckert, E. R. G., and R. M. Drake: Heat and Mass Transfer. McGraw-Hill Book Co., Inc., 1959, Chapter 8.

6. Patch, R. W.: Methods for Calculating Heat Transfer in High Temperature Hydrogen Gas. UAC Research Laboratories Report M-1492-1, November 1961.

7. Krascella, N. L.: Theoretical Investigation of the Absorptive Properties of Small Particles and Heavy Atom Gases. NASA CR-693, 1967. Unclassified.

8. Krascella, N. L.: Theoretical Investigation of the Opacity of Heavy Atom Gases. UAC Research Laboratories Report D-910092-4, September 1965. Unclassified.

9. Schlichting, H. S.: Boundary Layer Theory. McGraw-Hill Book Co., Inc., 4th ed., 1960, Chapter 23.

10. McLafferty, G. H., H. E. Bauer, and D. E. Sheldon: Preliminary Conceptual Design Study of a Specific Vortex-Stabilized Gaseous Nuclear Rocket Engine (U). NASA CR-698, 1967. (Report classified Confidential)

11. Krascella, N. L.: Tables of the Composition, Opacity, and Thermodynamic Properties of Hydrogen at High Temperatures. UAC Research Laboratories Report B-910168-1, September 1963. (Also issued as NASA SP-3005.)

12. Schneiderman, S. B.: High Temperature Viscosities and Diffusivities of Ionized Hydrogen-Uranium Mixtures. Third Conference on Performance of High Temperature Systems, December 1964.

13. Grier, N. T.: Calculation of Transport Properties and Heat Transfer Parameters of Dissociating Hydrogen, NASA TN D-1406, October 1962.

14. Taylor, G. I.: Internal Waves and Turbulence in a Fluid of Variable Density. The Scientific Papers of G. I. Taylor, Vol. II, Cambridge University Press, 1960.

15. Prandtl, L.: Einfluss stabilisierender Kräfte auf die Turbulenz. Vorträge auf dem Gebeite der Aerodynamik und verwandter Gebeite, Aachen, 1929. Also Gesammelte Abhandlungen, Part II, Springer-Verlag, 1961.

LIST OF SYMBOLS

a_P	Planck mean absorption coefficient, cm^{-1} or ft^{-1}
a_R	Rosseland mean absorption coefficient (see Eq. (7)), cm^{-1} or ft^{-1}
a_ω	Spectral absorption coefficient, cm^{-1}
a_ω^*	Value of a_ω corrected for stimulated emission factor (see Eq. (8)), cm^{-1}
$\bar{a}$	Flux mean absorption coefficient (see Eq. (10)), cm^{-1} or ft^{-1}
b	One quarter of jet diameter, in. or ft
B_ω	Spectral black-body radiation intensity, erg/cm^2-sec-steradian-cm^{-1}
c	Velocity of light, 3.0×10^{10} cm/sec
C_p	Specific heat, Btu/lb-deg R
d_j	Jet diameter (see Fig. 19), in. or ft
h	Planck constant, 6.62×10^{-27} erg/sec
H	Enthalpy, Btu/lb
k	Boltzmann constant, 1.379×10^{-16} erg/deg K
K_e	Effective thermal conductivity (see Eq. (14)), Btu/sec-ft-deg R
K_r	Radiation thermal conductivity (see Eq. (14)), Btu/sec-ft-deg R
K_t	Turbulent thermal conductivity (see Eq. (14)), Btu/sec-ft-deg R
M	Dimensionless temperature gradient (see Fig. 23)
n_R	Radiation attenuation parameter (see Eq. (12))
n_R'	Modified radiation attenuation parameter (see Eq. (9))
N_Γ	Exponent in circulation profile law (see Eq. (26)), dimensionless
P_T	Total pressure, atm

Q Total heat flux, Btu/sec-ft^2 or erg/sec-cm^2

Q_ω Spectral radiant heat flux, erg/cm^2-sec-cm^{-1}

r Distance from centerline of vortex tube, r_o denotes reference value, r_i denotes radius of vortex chamber, ft or cm

Ri Generalized Richardson number (see Eq. (24)), dimensionless

T Temperature, deg R or deg K

U Jet centerline velocity, ft/sec

V_j Jet injection velocity (see Fig. 19), ft/sec

V_ϕ Tangential component of propellant velocity, ft/sec

V_z Axial component of propellant velocity, ft/sec

W_R Radial flow rate of hydrogen propellant, lb/sec-ft^2

x Distance from peripheral wall (see Fig. 1), ft or cm

y Distance from position at which propellant temperature equals 60,000 R (see Fig. 1), ft or cm

α Molecular heat diffusivity, ft^2/sec

Γ Circulation, rV_ϕ, Γ_o denotes reference value, ft^2/sec

ϵ_α Turbulent heat diffusivity, ft^2/sec

ϵ_{α_o} Value of ϵ_α evaluated for $Ri = 0$, ft^2/sec

ϵ_ν Turbulent kinematic viscosity, ft^2/sec

μ Viscosity, lb/ft-sec

ν Molecular kinematic viscosity, ft^2/sec

ρ Density, lb/ft^3

σ Stefan-Boltzmann constant, 0.48×10^{-12} Btu/sec-ft^2-(deg R)^4

ω Wave number, cm^{-1}

FIG. 1

FLOW PATTERN ASSUMED IN ANALYSIS OF TEMPERATURE DISTRIBUTION

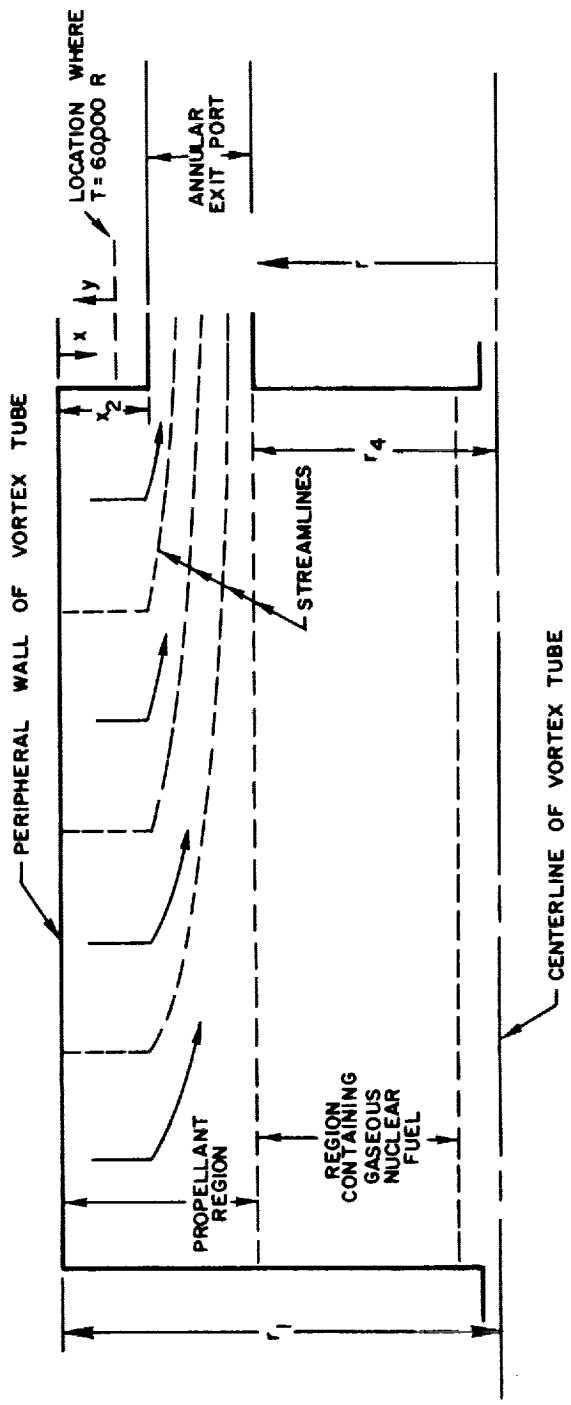

FIG. 2

EFFECT OF WAVE NUMBER ON SPECTRAL ABSORPTION COEFFICIENT OF SOLID TUNGSTEN SEED

TUNGSTEN DENSITY AT EACH TEMPERATURE EQUAL TO 3% OF THAT OF HYDROGEN AT A PRESSURE OF 1000 ATM

CURVE	DESCRIPTION
———	FROM REF. 7 ; USED IN PRESENT CALCULATIONS
— — — —	FROM REF. 8 ; USED IN CALCULATIONS OF REF. 4

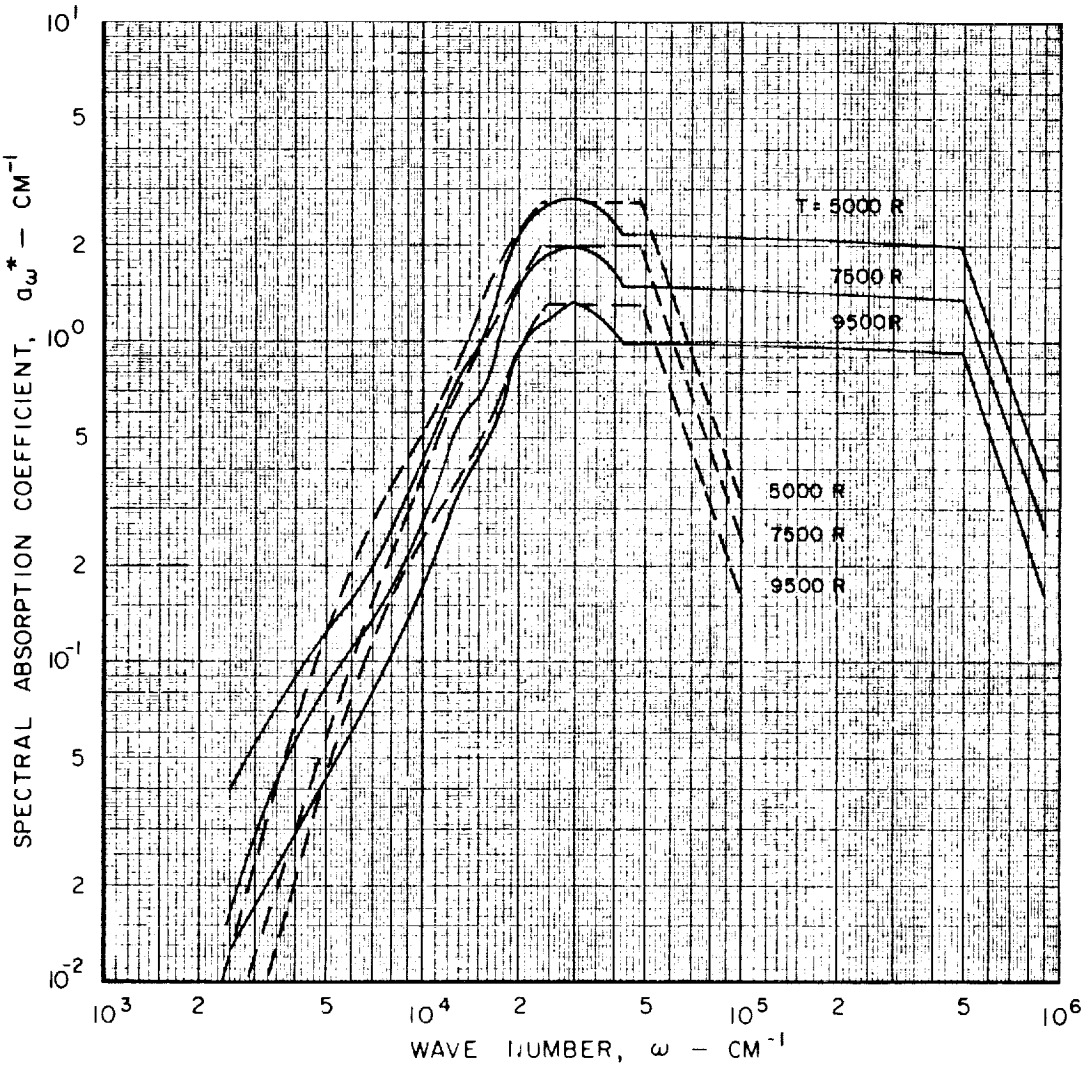

FIG. 3

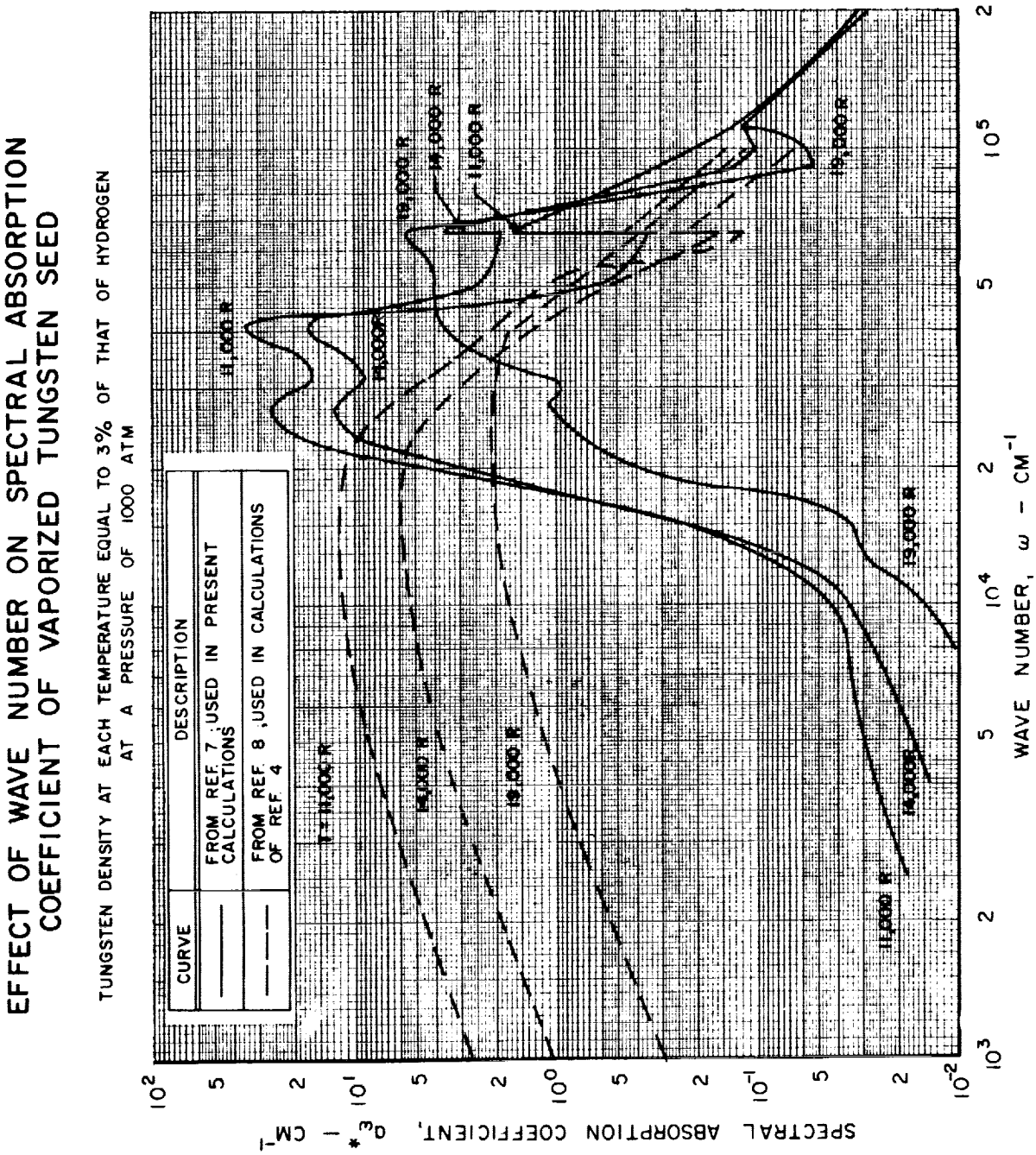
EFFECT OF WAVE NUMBER ON SPECTRAL ABSORPTION COEFFICIENT OF VAPORIZED TUNGSTEN SEED
TUNGSTEN DENSITY AT EACH TEMPERATURE EQUAL TO 3% OF THAT OF HYDROGEN AT A PRESSURE OF 1000 ATM
CURVE
DESCRIPTION
FROM REF. 7 ; USED IN PRESENT CALCULATIONS
FROM REF. 8 ; USED IN CALCULATIONS OF REF. 4
T = 11,000 °R
14,000 °R
19,000 °R
11,000 °R
14,000 °R
19,000 °R
SPECTRAL ABSORPTION COEFFICIENT, α_ω^* - CM^{-1}
WAVE NUMBER, ω - CM^{-1}

FIG. 4

EFFECT OF WAVE NUMBER ON THE TOTAL SPECTRAL ABSORPTION COEFFICIENT OF MIXTURE OF HYDROGEN AND TUNGSTEN SEED

$\frac{\rho \text{ TUNGSTEN}}{\rho \text{ HYDROGEN}} = 0.03$ $\quad P_T = 1000$ ATM

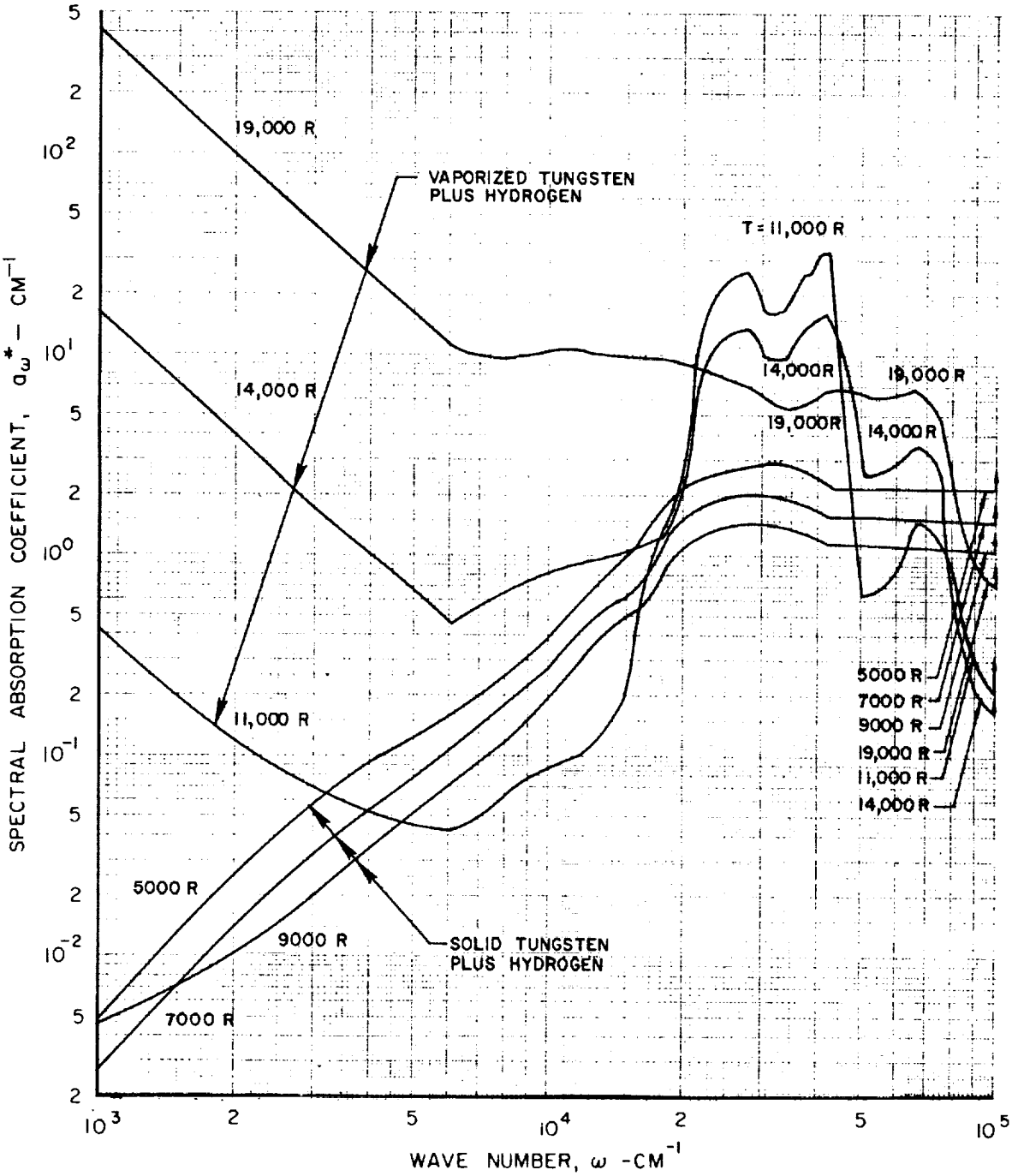

FIG. 5

COMPARISON OF SPECTRAL ABSORPTION COEFFICIENTS OF MIXTURES OF HYDROGEN AND TUNGSTEN SEED USED IN PRESENT AND PRECEDING CALCULATIONS

$\frac{\rho \text{ TUNGSTEN}}{\rho \text{ HYDROGEN}} = 0.03$ $\quad P_T = 1000$ ATM

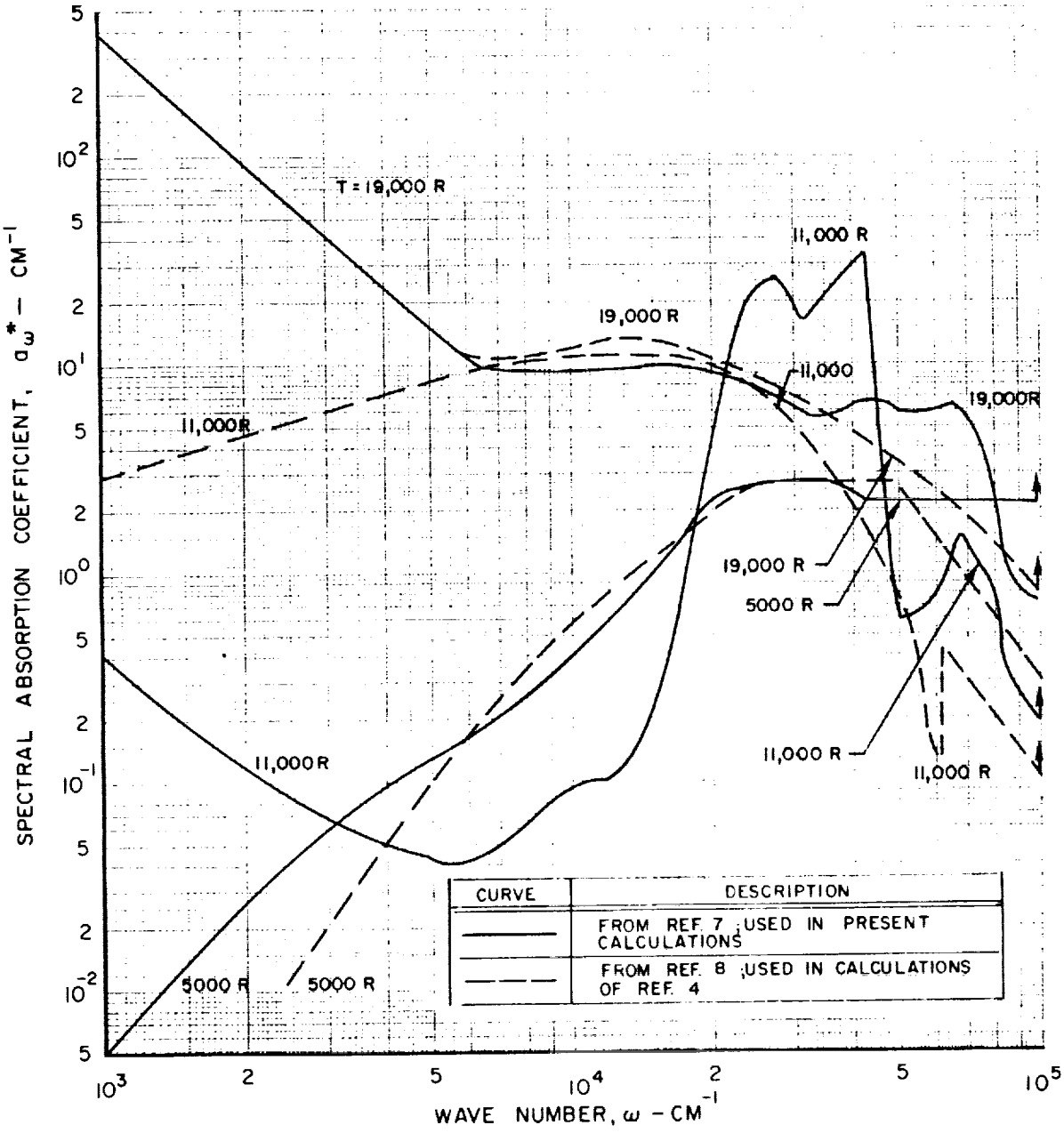

FIG. 6

EFFECT OF TEMPERATURE ON ROSSELAND MEAN OPACITY OF MIXTURE OF HYDROGEN AND TUNGSTEN SEED

$\frac{\rho_{TUNGSTEN}}{\rho_{HYDROGEN}} = 0.03$ $\quad P_T = 1000$ ATM

CURVE	DESCRIPTION
———	FROM REF. 7 ; USED IN PRESENT CALCULATIONS
– – – –	FROM REF. 8 ; USED IN CALCULATIONS OF REF. 4

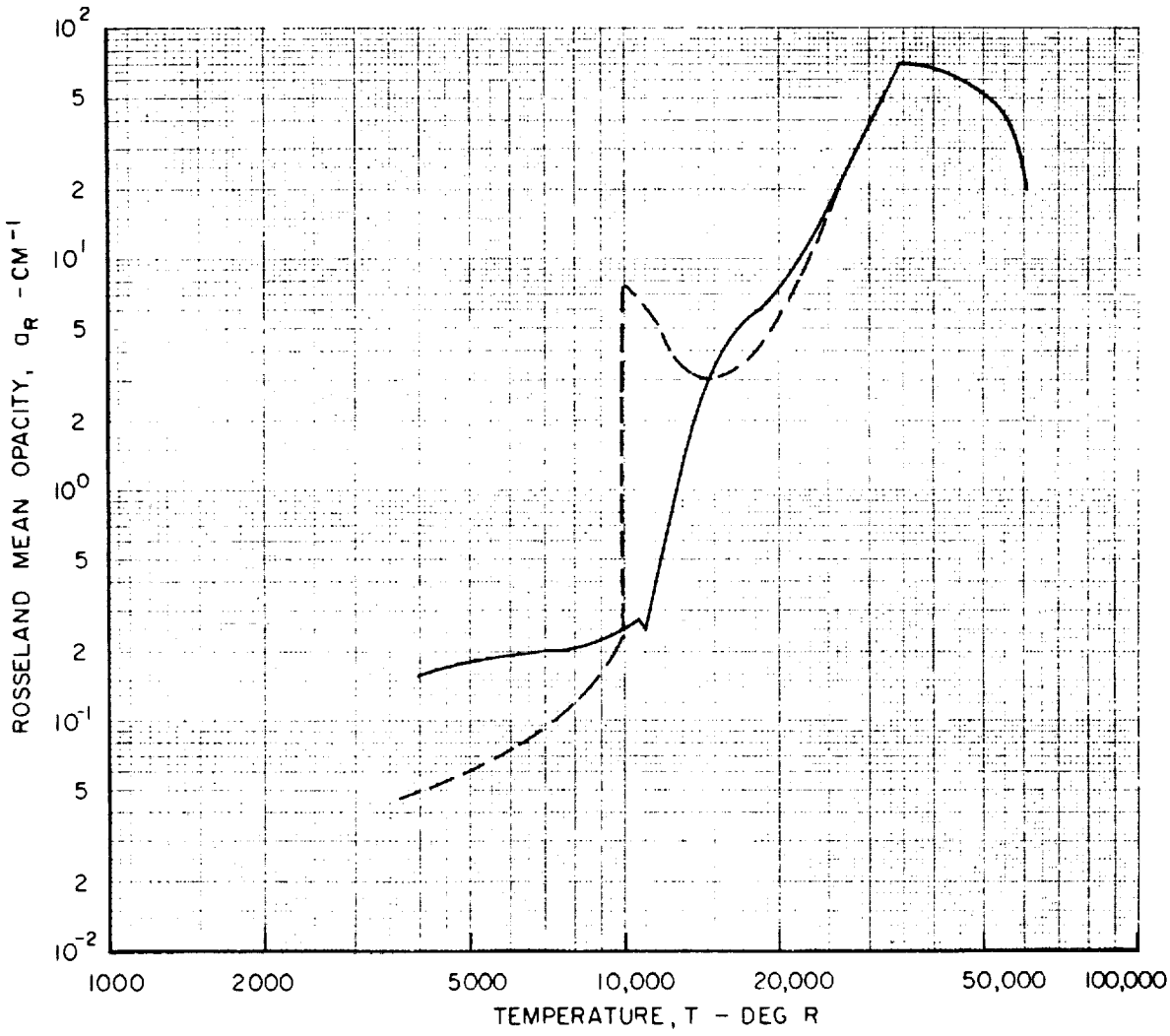

FIG. 7

COMPARISON OF ROSSELAND MEAN OPACITY AND SPECTRAL ABSORPTION COEFFICIENT OF MIXTURE OF HYDROGEN AND TUNGSTEN SEED

$\frac{\rho_{TUNGSTEN}}{\rho_{HYDROGEN}} = 0.03$ $\quad P_T = 1000$ ATM

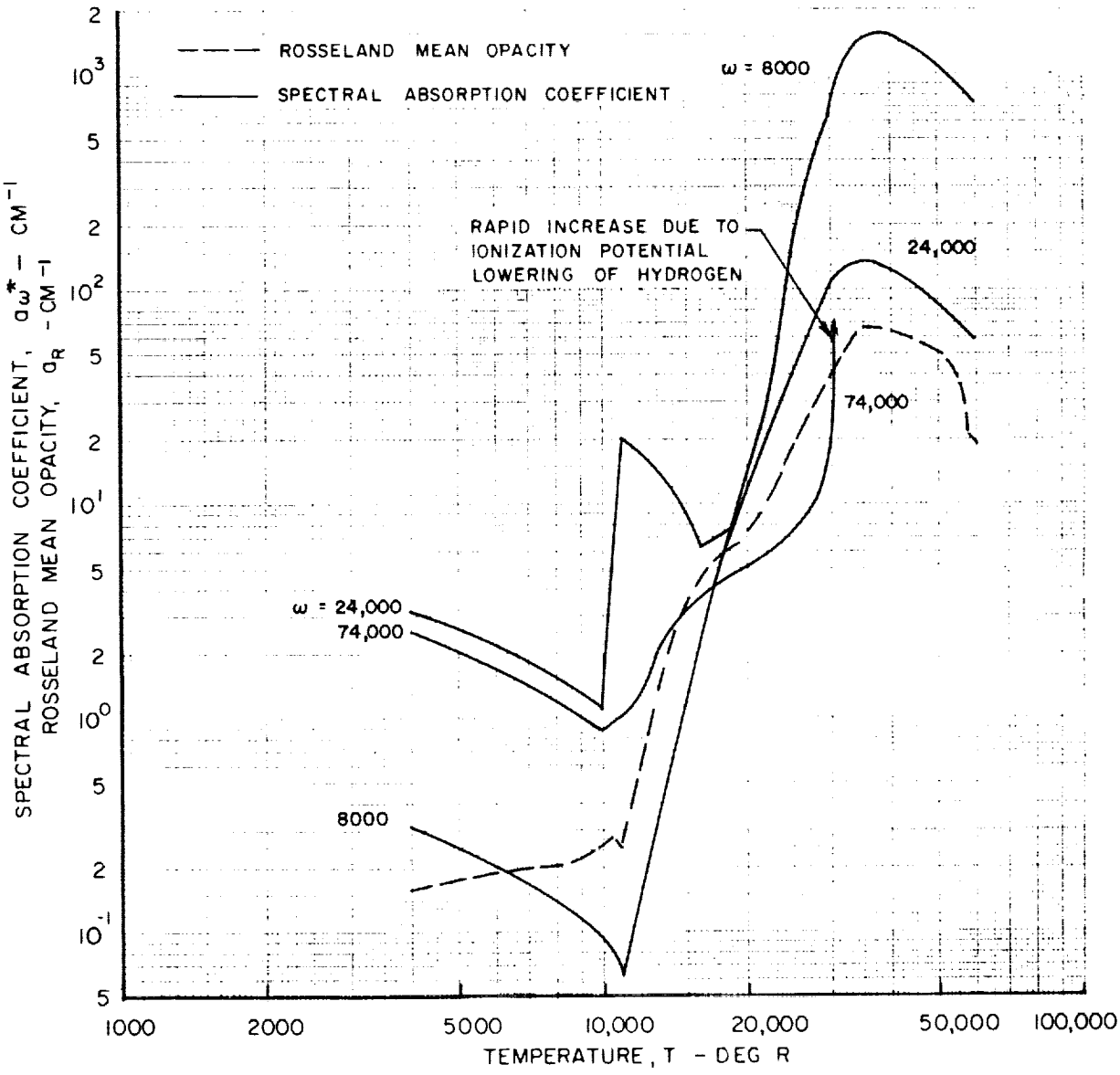

FIG. 8

VARIATION OF TOTAL HEAT FLUX WITH TEMPERATURE IN THE PROPELLANT REGION FOR DIFFERENT HYDROGEN RADIAL WEIGHT FLOWS

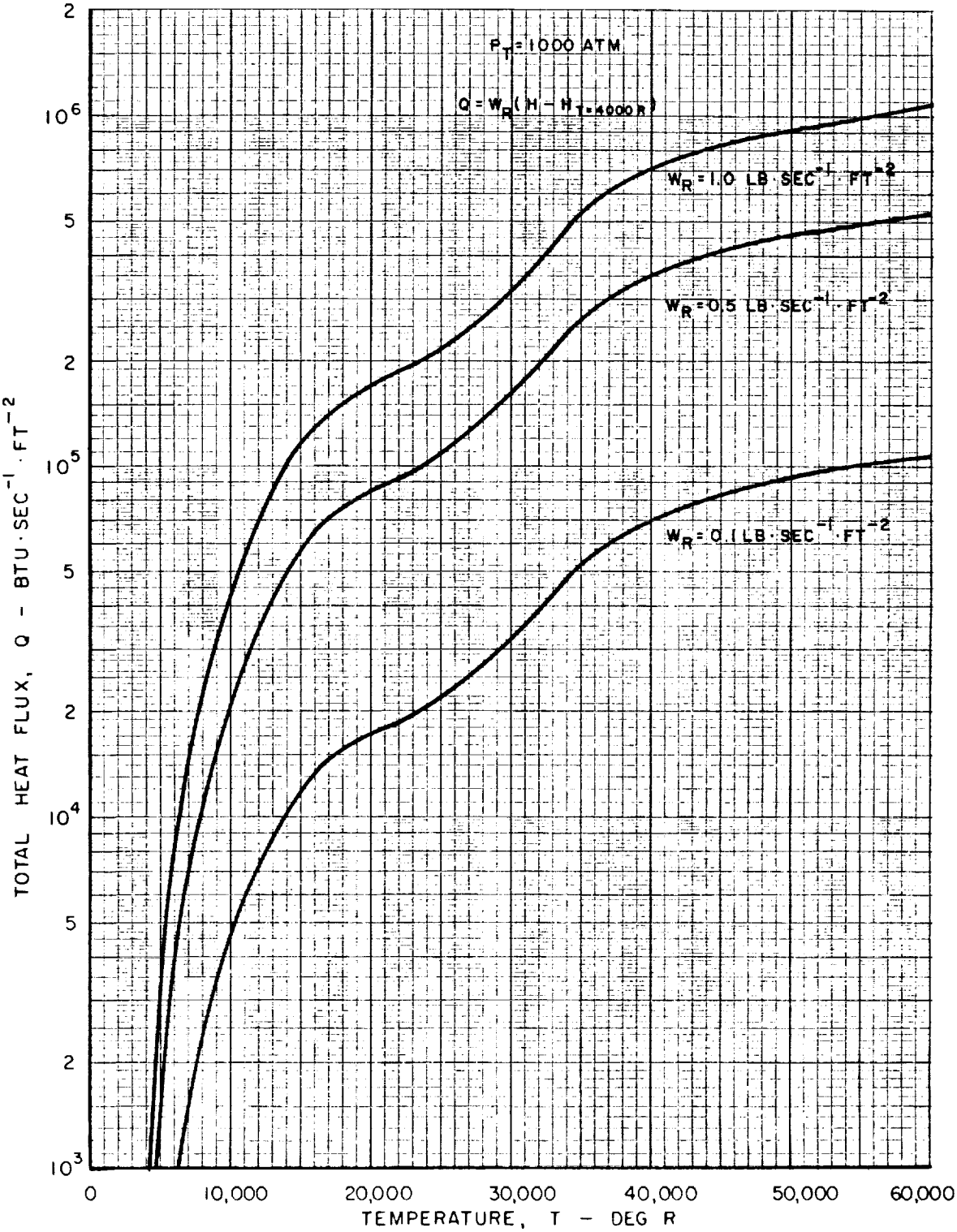

FIG. 9

RADIATION ATTENUATION PARAMETER DETERMINED FOR DIFFERENT PROPELLANT RADIAL WEIGHT FLOWS

CURVE	DESCRIPTION	RADIAL WEIGHT FLOW LB·SEC^{-1}·FT^{-2}
———	DETERMINED FROM PRESENT CALCULATIONS	1.0
—— – ——	DETERMINED FROM PRESENT CALCULATIONS	0.5
– – – –	DETERMINED FROM PREVIOUS CALCULATIONS IN REF. 4	1.0

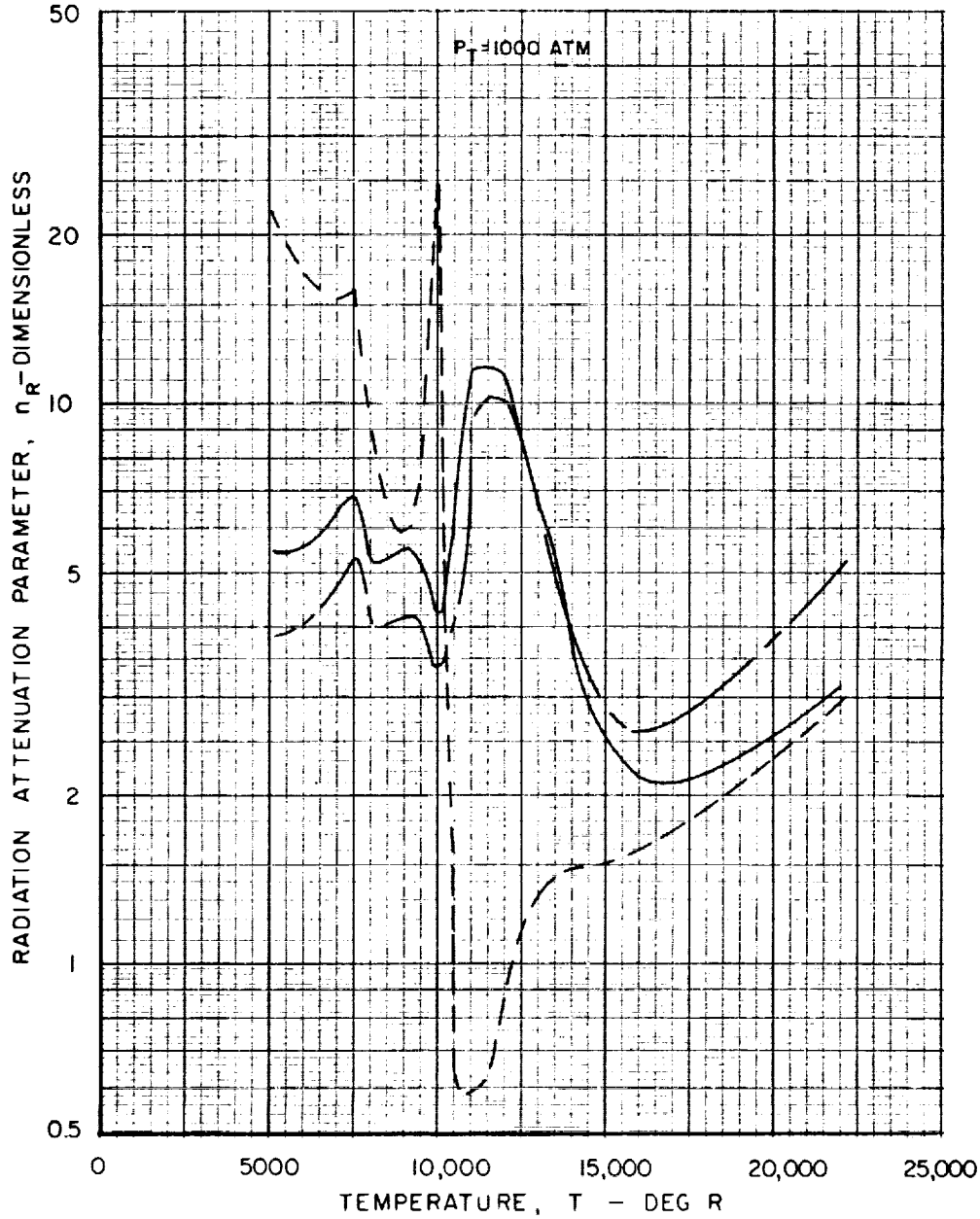

FIG. 10

CALCULATED TEMPERATURE DISTRIBUTIONS FOR DIFFERENT PROPELLANT RADIAL WEIGHT FLOWS

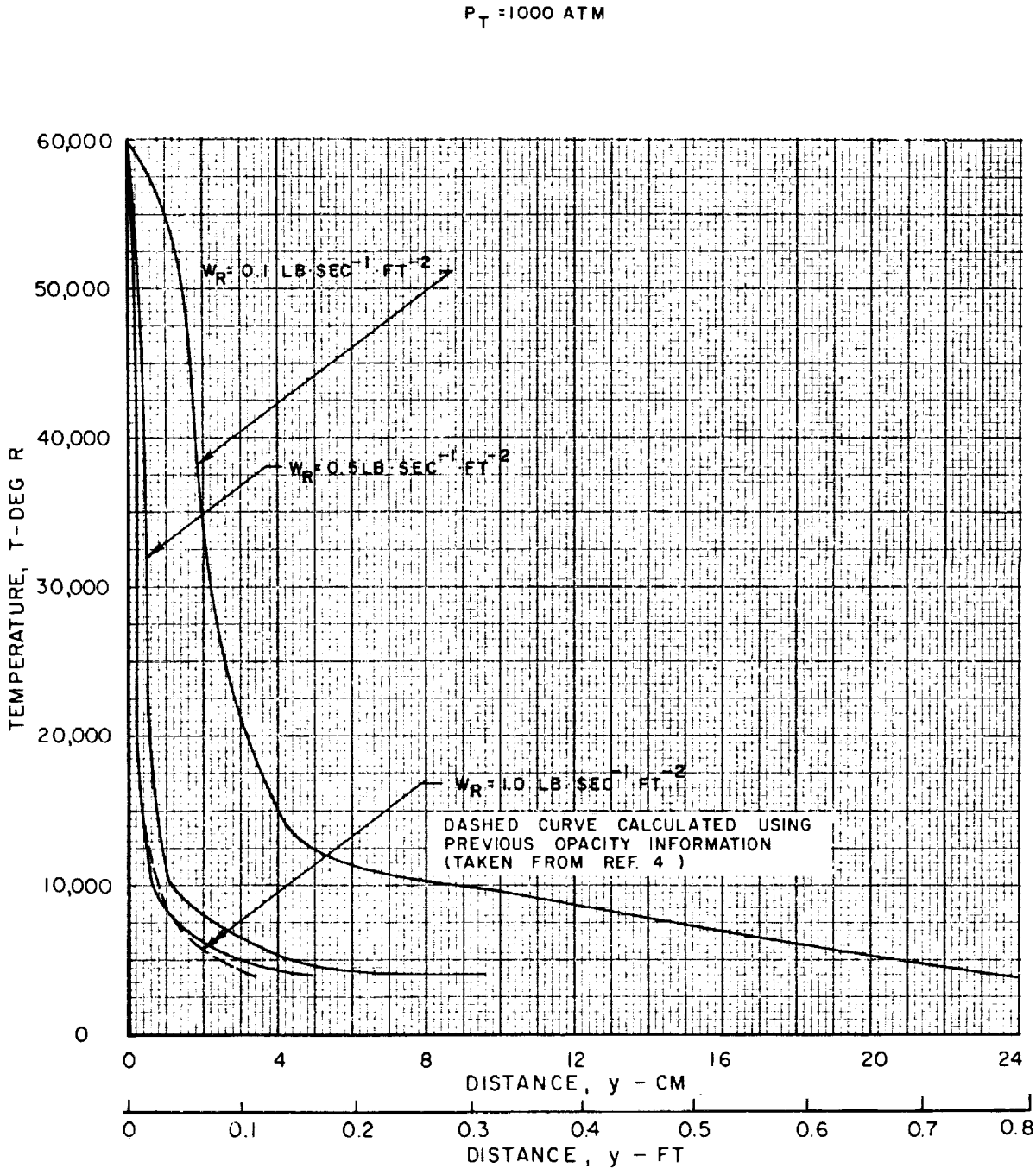

FIG. 11

VARIATION OF SPECTRAL HEAT FLUX WITH WAVE NUMBER FOR HYDROGEN RADIAL WEIGHT FLOW OF 1.0 LB · SEC^{-1} · FT^{-2}

P_T = 1000 ATM

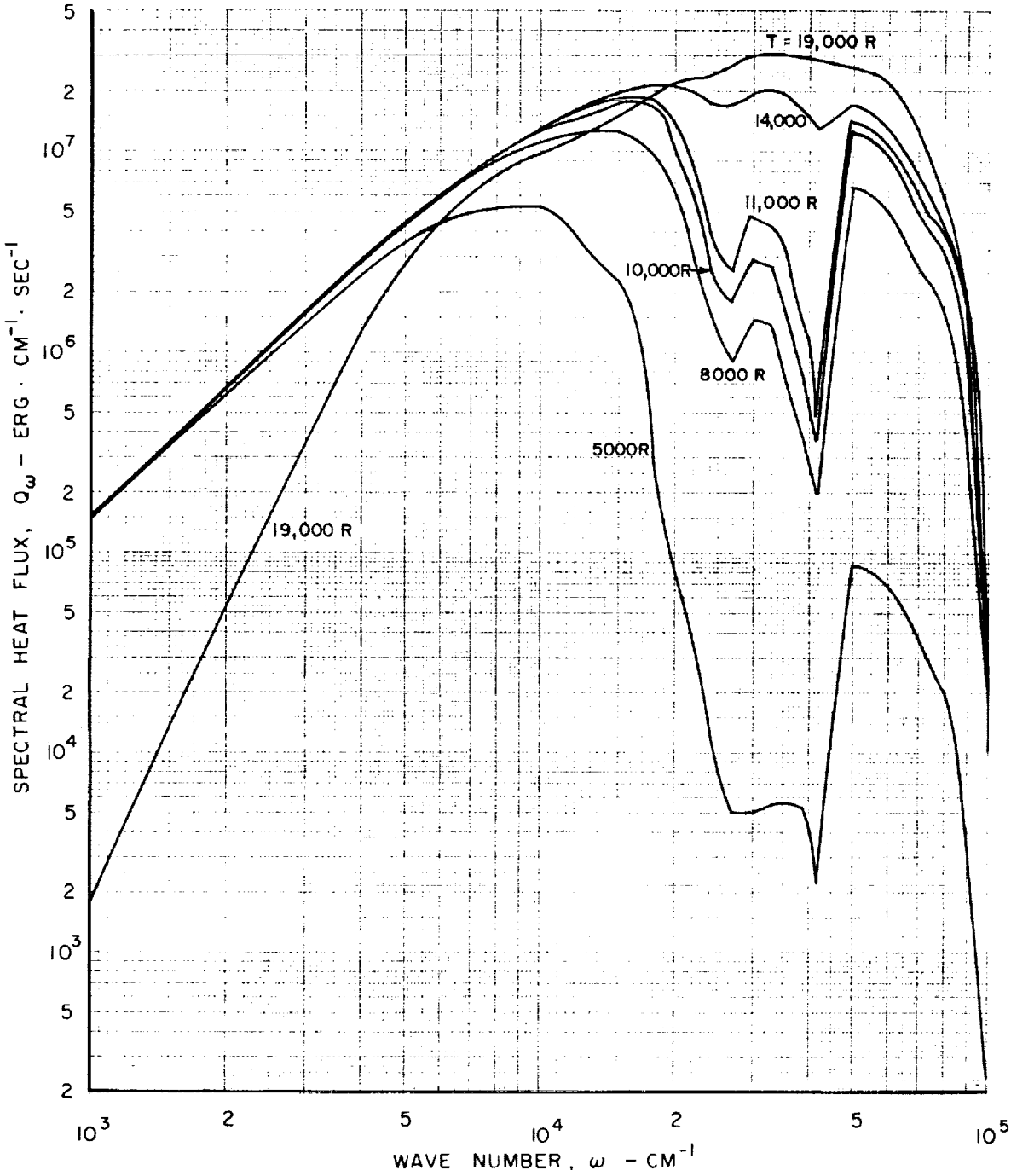

FIG. 12

VARIATION OF SPECTRAL HEAT FLUX WITH WAVE NUMBER FOR HYDROGEN RADIAL WEIGHT FLOW OF 0.5 LB · SEC^{-1} · FT^{-2}

P_T = 1000 ATM

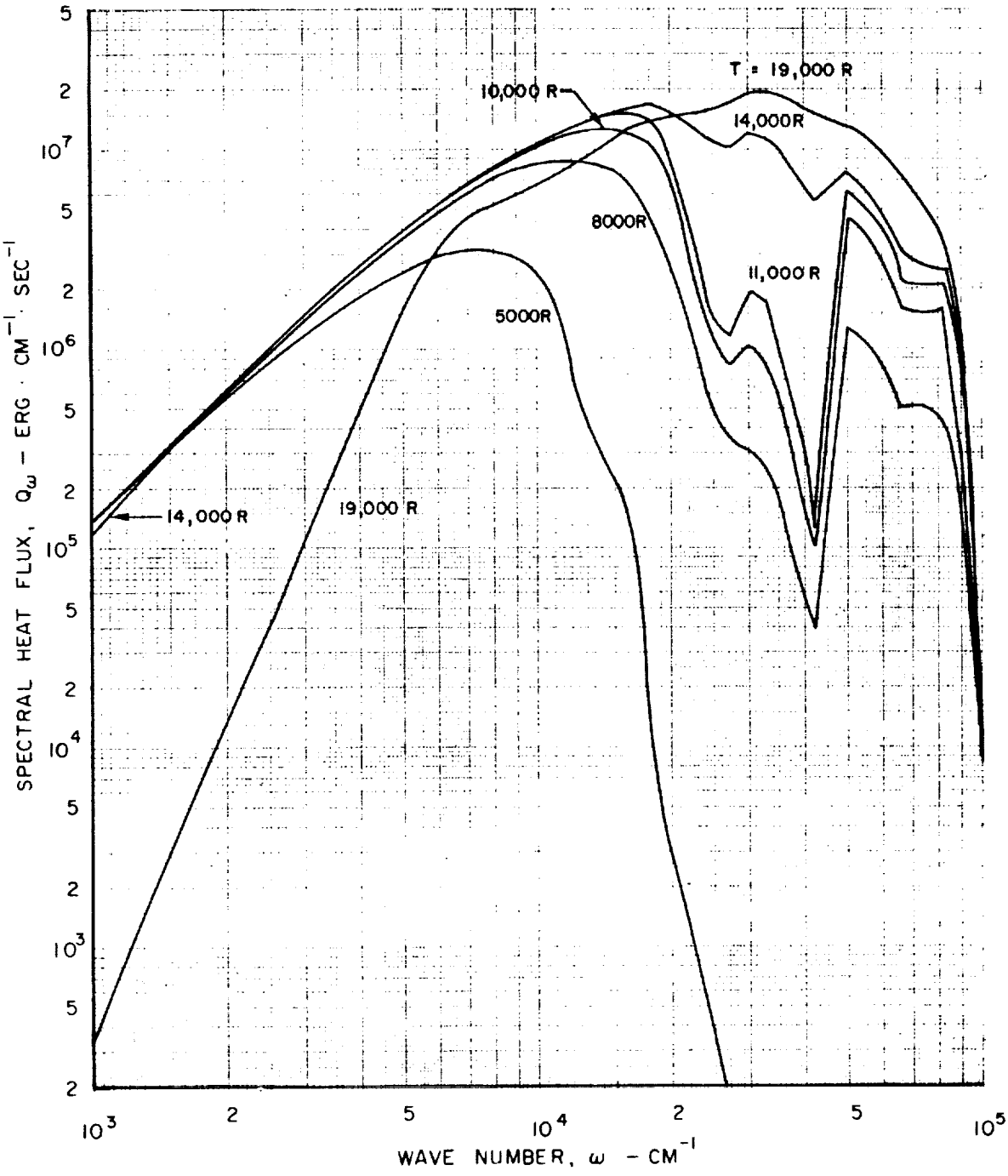

FIG. 13

VARIATION OF SPECTRAL HEAT FLUX WITH WAVE NUMBER FOR HYDROGEN RADIAL WEIGHT FLOW OF 0.1 LB · SEC^{-1} · FT^{-2}

P_T = 1000 ATM

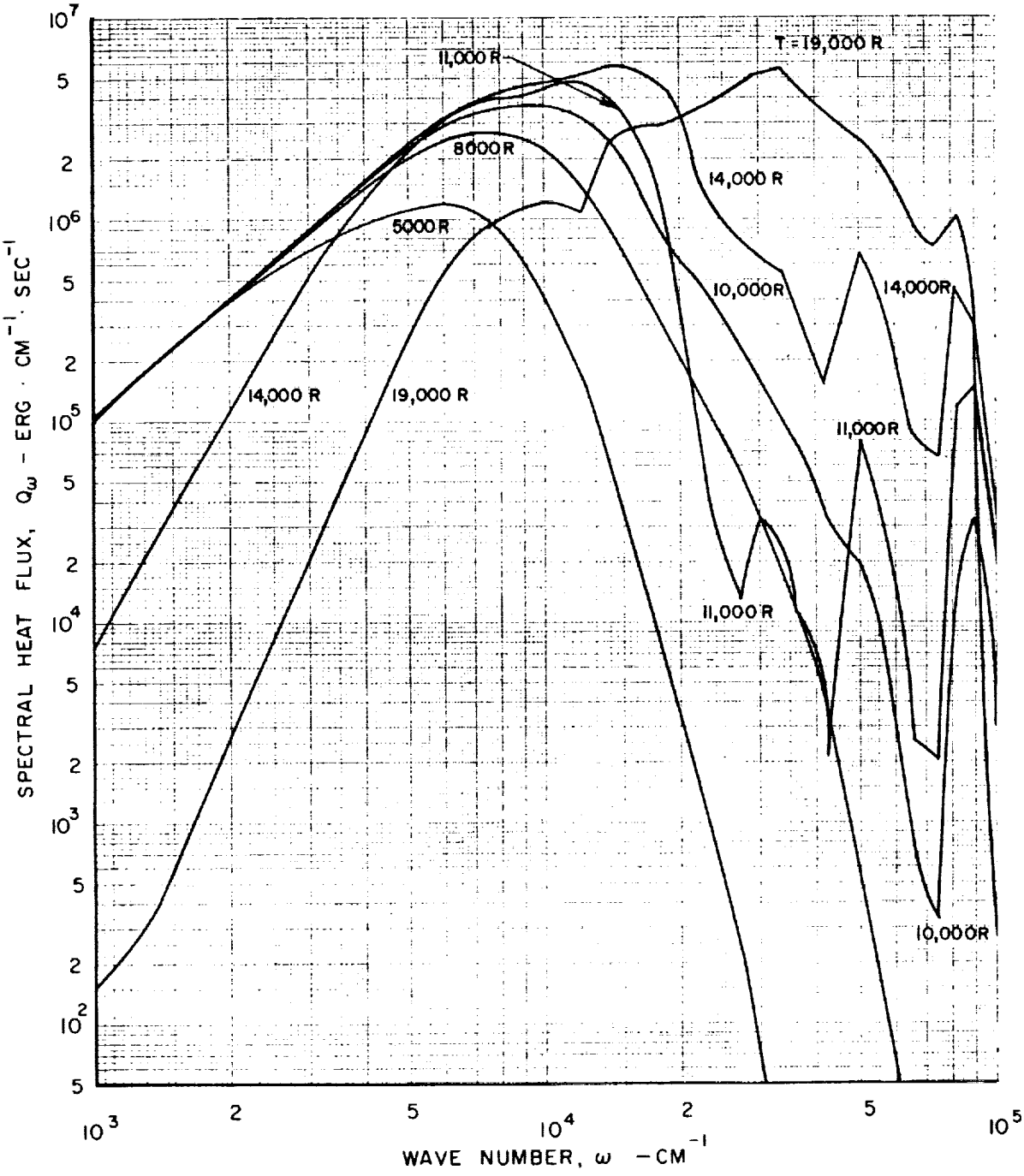

FIG. 14

COMPARISON OF TOTAL HEAT FLUX DISTRIBUTIONS AS CALCULATED FROM MAIN AND SIMPLIFIED COMPUTER PROGRAMS FOR A PROPELLANT RADIAL WEIGHT FLOW OF 1.0 LB·SEC^{-1}·FT^{-2}

P_T = 1000 ATM

NOTE: SYMBOLS REPRESENT CALCULATED POINTS OBTAINED FROM MAIN COMPUTER PROGRAM

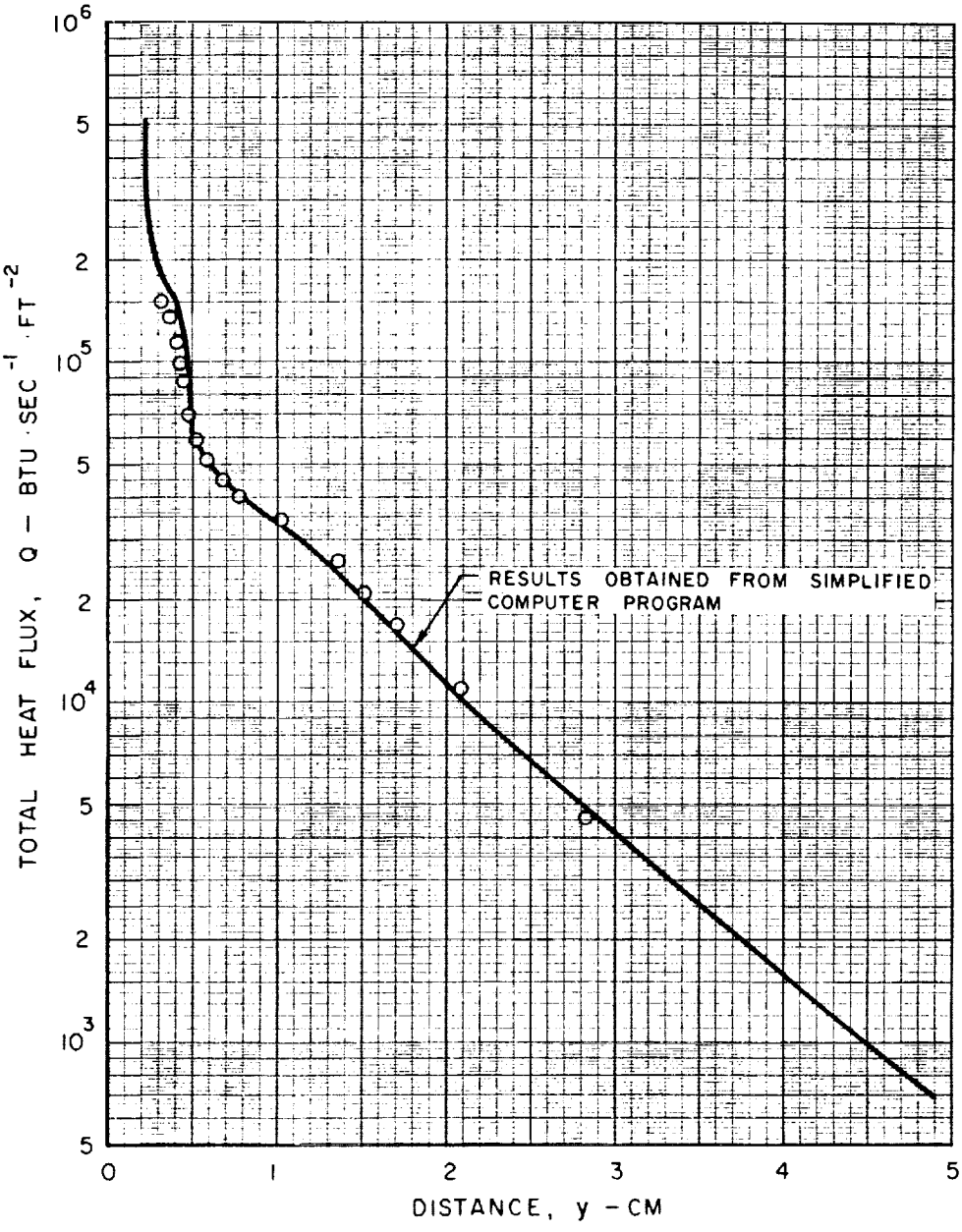

FIG. 15

COMPARISON OF TOTAL HEAT FLUX DISTRIBUTIONS AS CALCULATED FROM MAIN AND SIMPLIFIED COMPUTER PROGRAMS FOR A PROPELLANT RADIAL WEIGHT FLOW OF 0.5 LB·SEC^{-1}·FT^{-2}

P_T = 1000 ATM

NOTE : SYMBOLS REPRESENT CALCULATED POINTS OBTAINED FROM MAIN COMPUTER PROGRAM

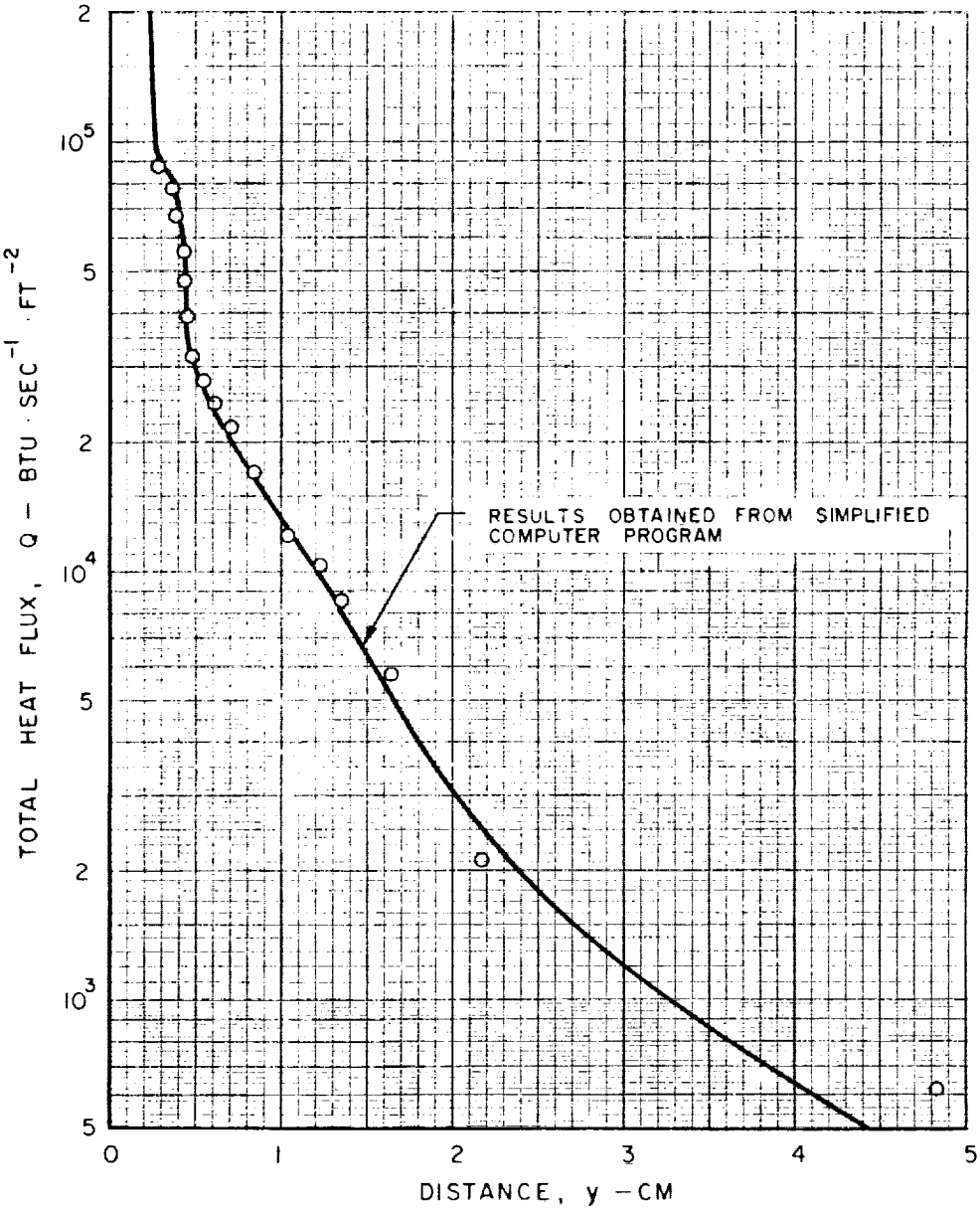

FIG. 16

COMPARISON OF TOTAL HEAT FLUX DISTRIBUTIONS AS CALCULATED FROM MAIN AND SIMPLIFIED COMPUTER PROGRAMS FOR A PROPELLANT RADIAL WEIGHT FLOW OF 0.1 LB·SEC^{-1}·FT^{-2}

P_T = 1000 ATM

NOTE : SYMBOLS REPRESENT CALCULATED POINTS OBTAINED FROM MAIN COMPUTER PROGRAM

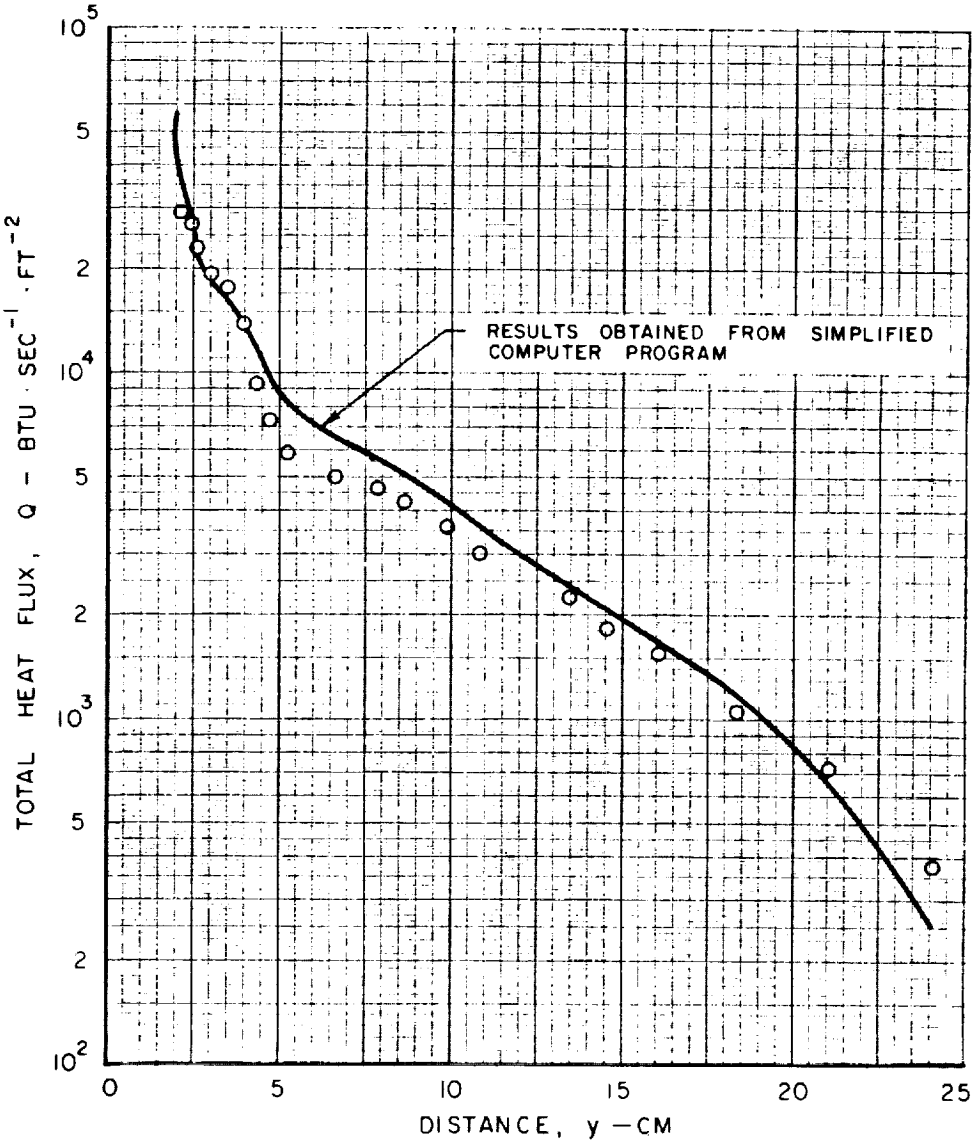

FIG. 17

COMPARISON OF FLUX MEAN ABSORPTION COEFFICIENTS AND ROSSELAND MEAN OPACITY

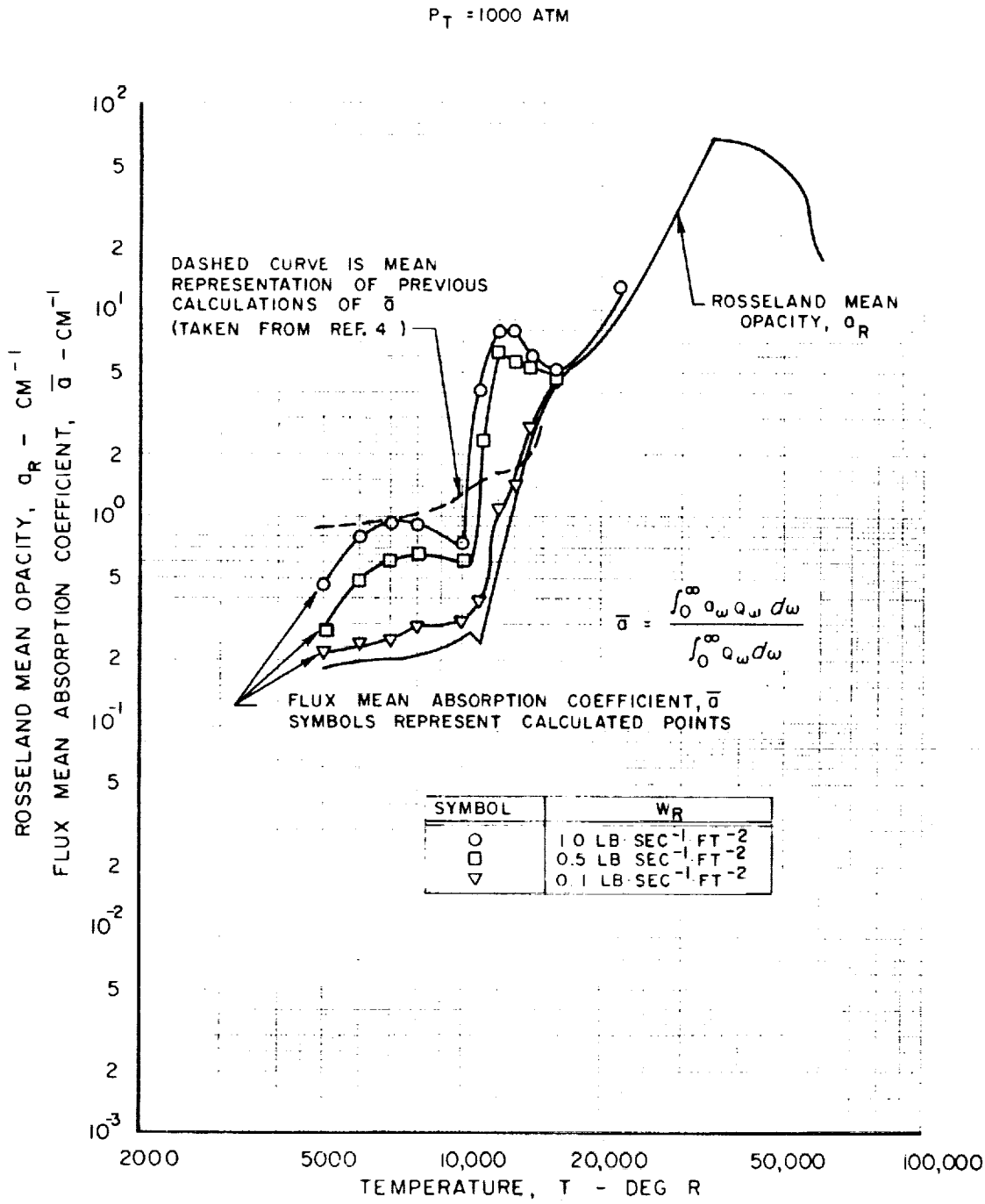

FIG. 18

EFFECT OF TEMPERATURE ON MODIFIED RADIATION ATTENUATION PARAMETER FOR DIFFERENT PROPELLANT RADIAL WEIGHT FLOWS

P_T = 1000 ATM

$$n_R' = \frac{n_R a_R}{\bar{a}}$$

SYMBOL	W_R
○	1.0 LB $SEC^{-1} \cdot FT^{-2}$
□	0.5 LB $SEC^{-1} \cdot FT^{-2}$

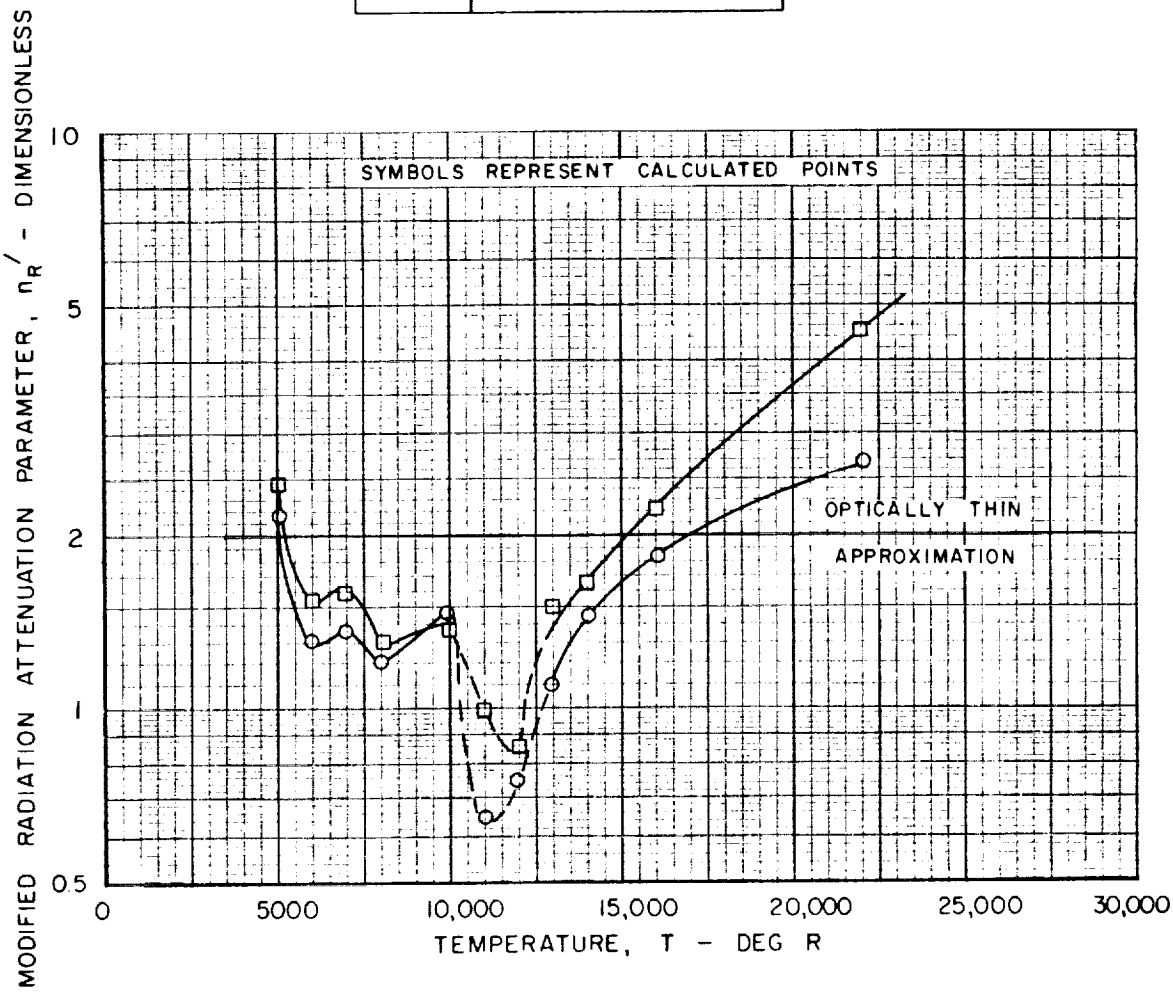

FIG. 19

EFFECT OF INJECTION VELOCITY AND JET DIAMETER ON TURBULENT KINEMATIC VISCOSITY AT EXIT OF INJECTION PORT

NOTE: DESIGN VALUES OF JET DIAMETER AND INJECTION VELOCITY OBTAINED FROM REF. 10

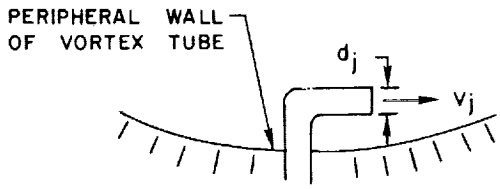

$\epsilon_\nu = 0.000533\ d_j\ v_j$ (SEE TEXT)

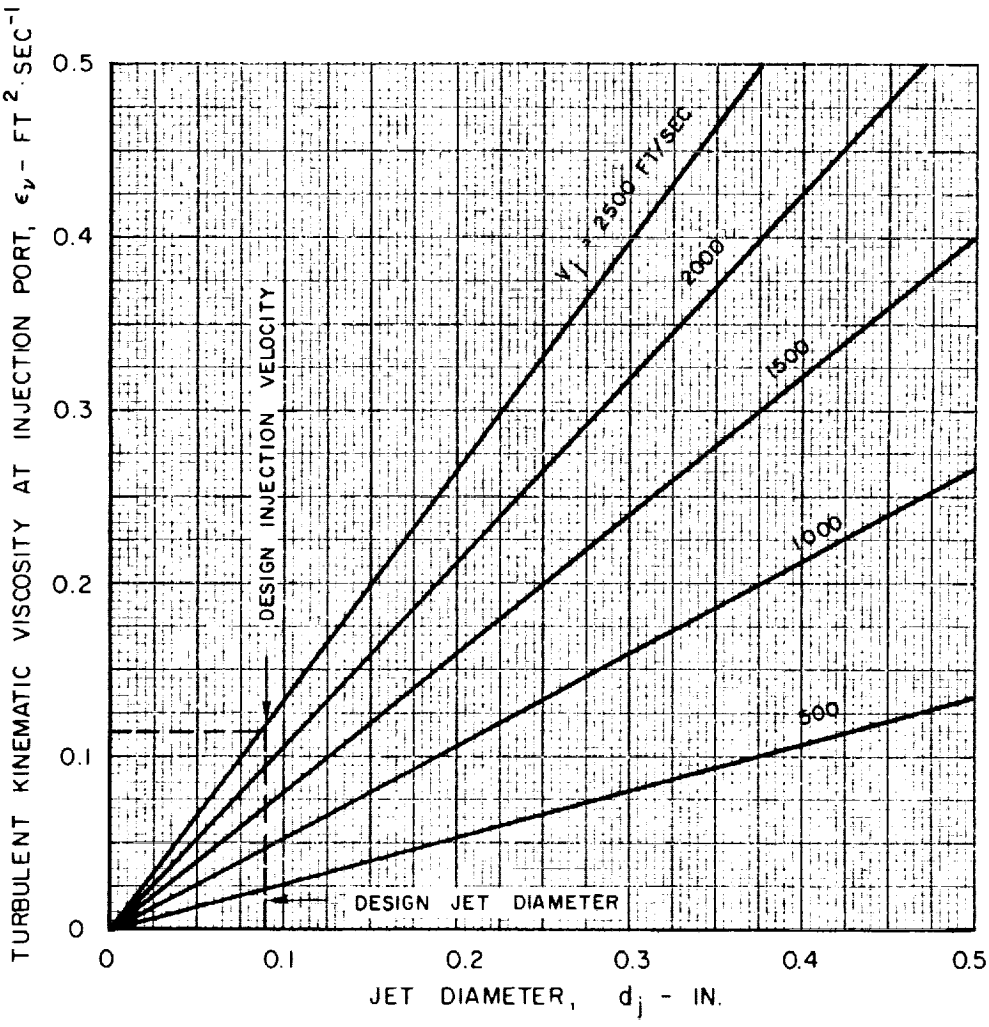

FIG. 20

EFFECT OF TEMPERATURE ON THE RATIO OF TURBULENT TO MOLECULAR KINEMATIC VISCOSITIES OF PROPELLANT

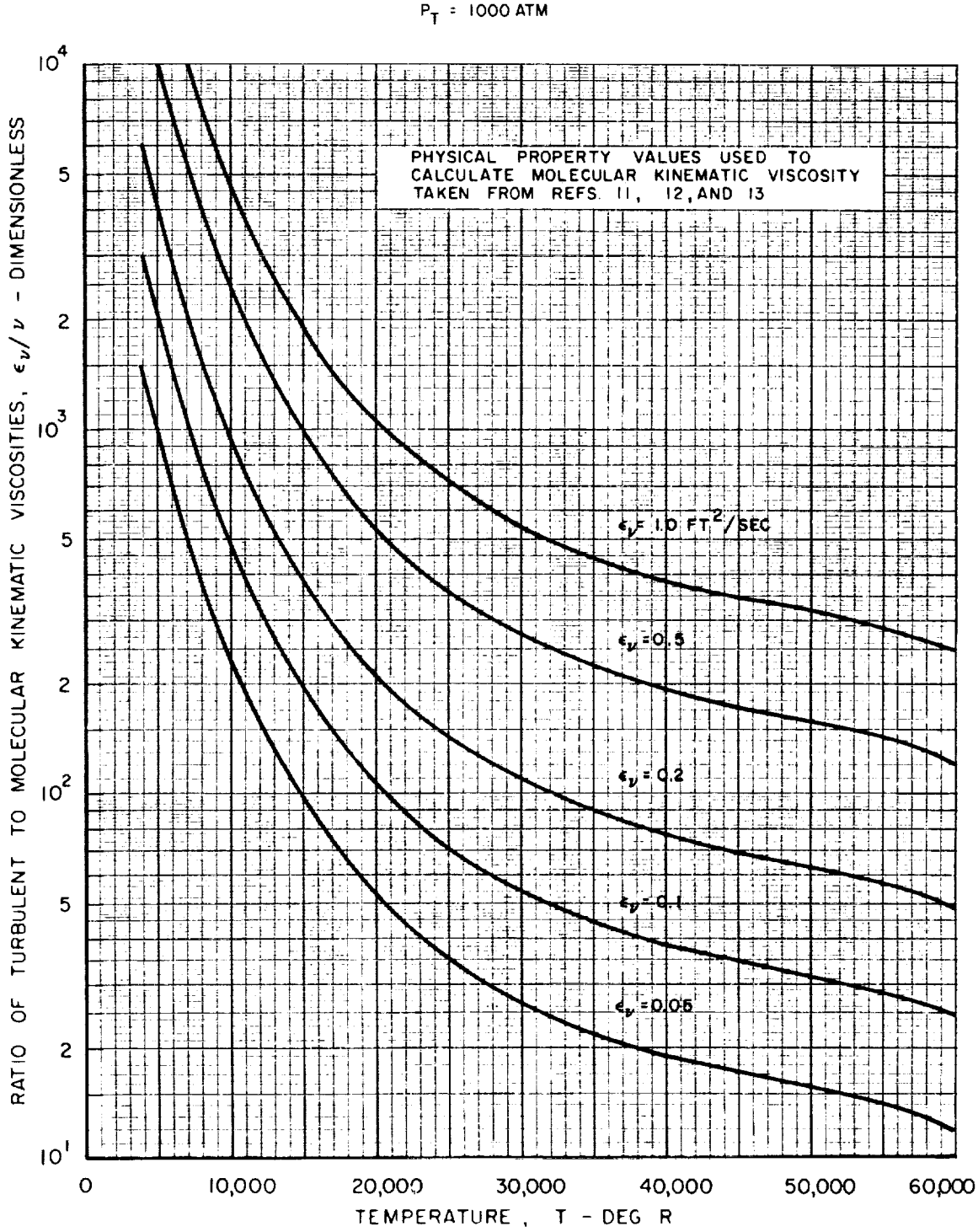

FIG. 21

EFFECT OF TEMPERATURE ON RADIATION AND TURBULENT THERMAL CONDUCTIVITIES OF PROPELLANT

P_T = 1000 ATM

NOTE: VALUES OF a_R TAKEN FROM FIG. 6
VALUES OF ρC_p TAKEN FROM FIG. 22

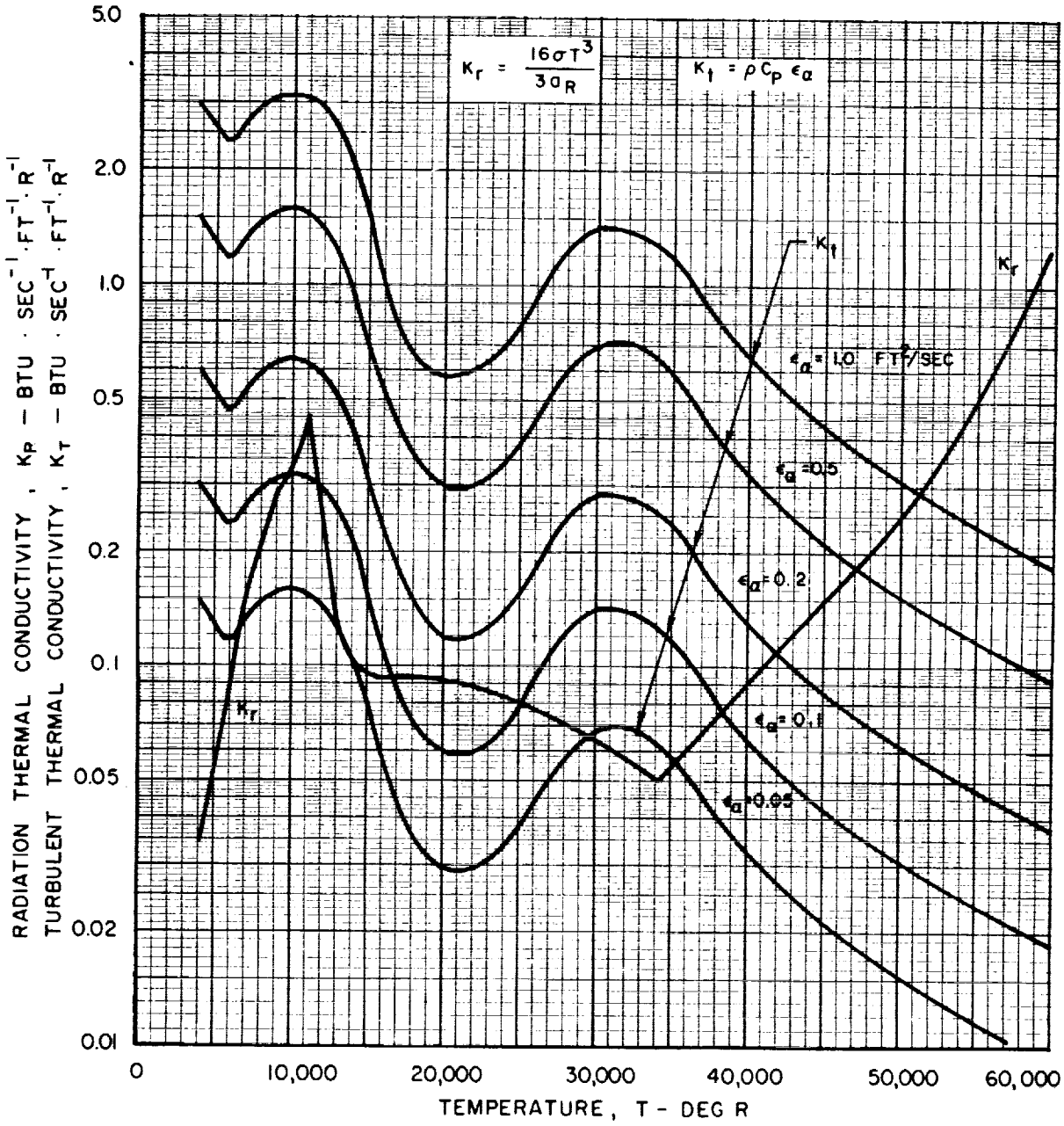

[redacted]

FIG. 22

EFFECT OF TEMPERATURE ON PHYSICAL PROPERTIES USED IN TURBULENCE CALCULATIONS

P_T = 1000 ATM

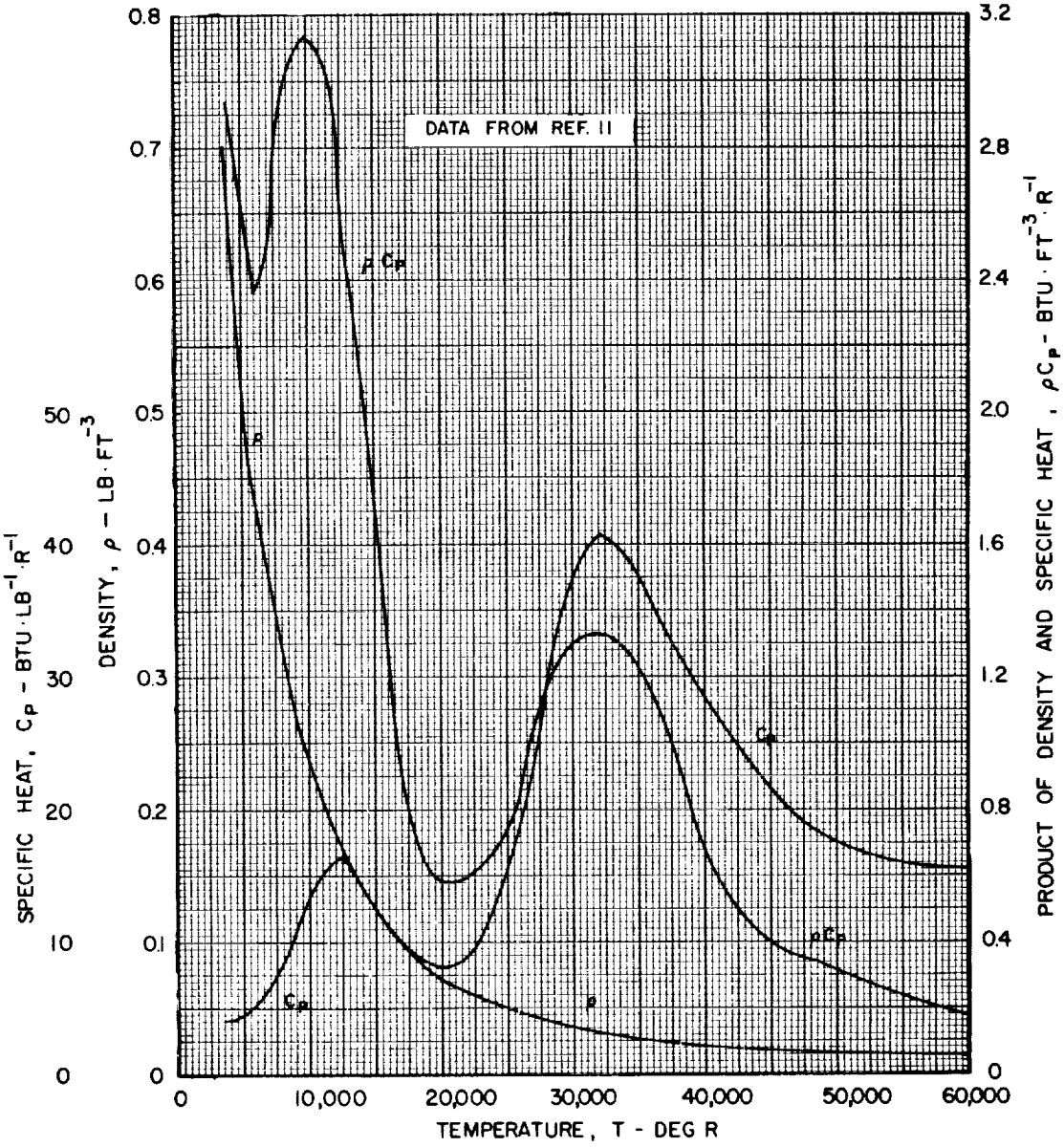

FIG. 23

EFFECT OF DIMENSIONLESS TEMPERATURE GRADIENT AND EXPONENT IN CIRCULATION PROFILE LAW ON GENERALIZED RICHARDSON NUMBER

$$\frac{\Gamma}{\Gamma_0} = \left(\frac{r}{r_0}\right)^{N_\Gamma}$$

$$M = -\frac{r}{T}\frac{dT}{dr}$$

$$Ri = \frac{M + 2N_\Gamma}{(N_\Gamma - 2)^2}$$

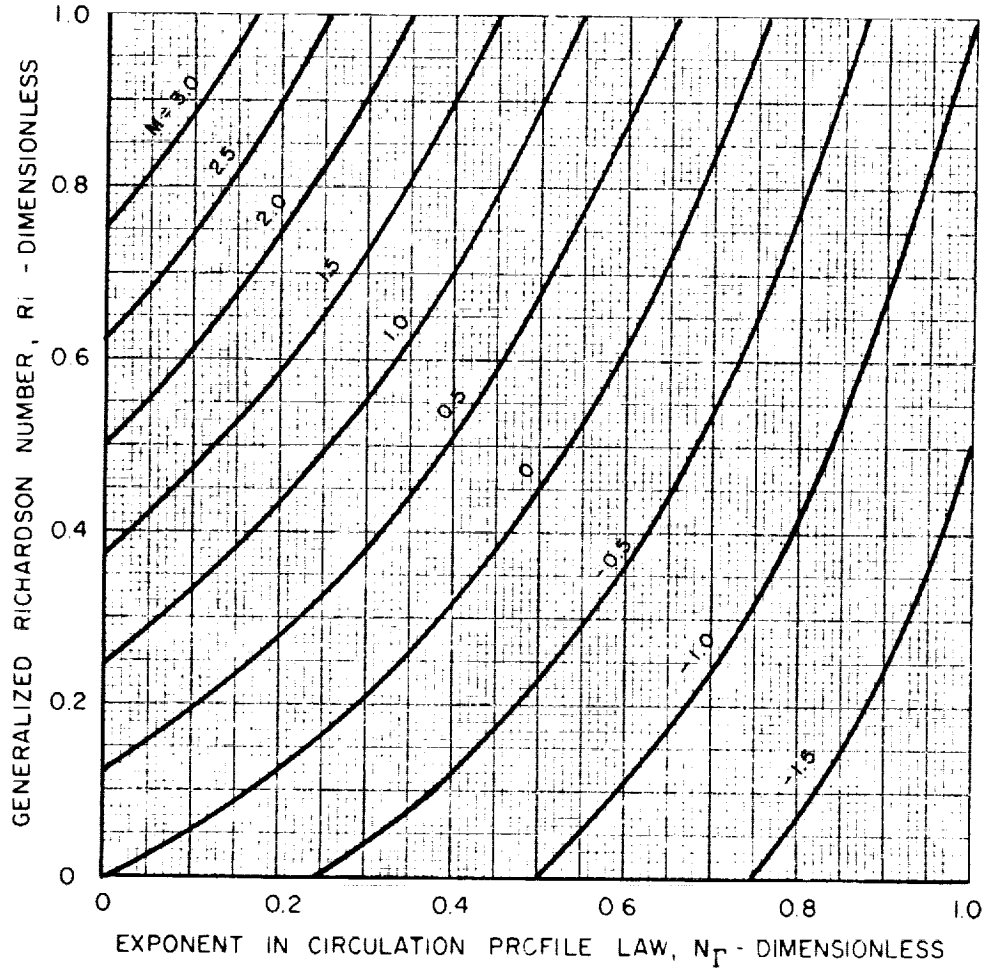

FIG. 24

ASSUMED EFFECT OF RICHARDSON NUMBER ON TURBULENT HEAT DIFFUSIVITY

$$\epsilon_a = \epsilon_{a_0} (1 - Ri)^{1/2}$$

NOTE: ϵ_{a_0} IS VALUE DETERMINED FOR Ri=0

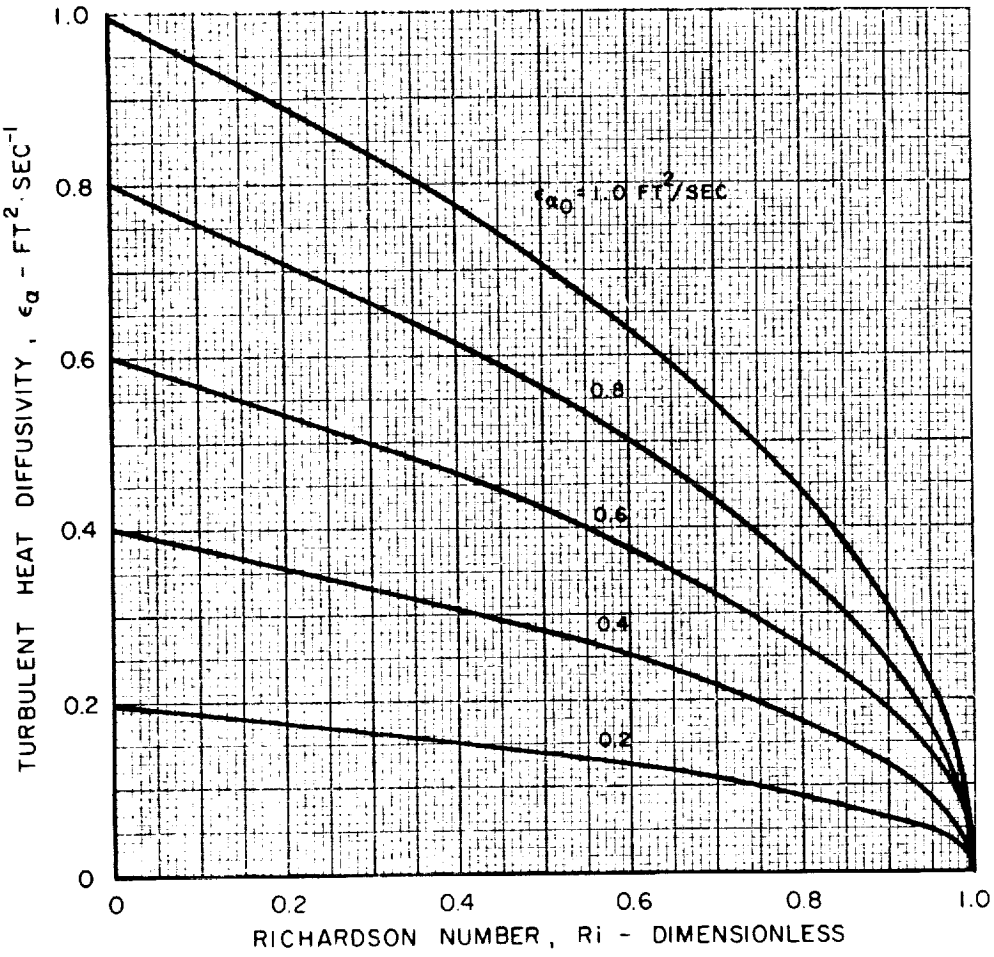

FIG. 25

TYPICAL TEMPERATURE PROFILES IN PERIPHERAL WALL REGION INCLUDING THE EFFECTS OF TURBULENCE

$N_\Gamma = 0$

$r_1 = 100$ CM

$W_R = 1.0$ LB·SEC^{-1}·FT^{-2}

TEMPERATURES CALCULATED USING OPTICALLY THICK APPROXIMATION

ARROWS ON CURVES DENOTE POINT WHERE TURBULENCE DISAPPEARS DUE TO RICHARDSON NUMBER EXCEEDING UNITY

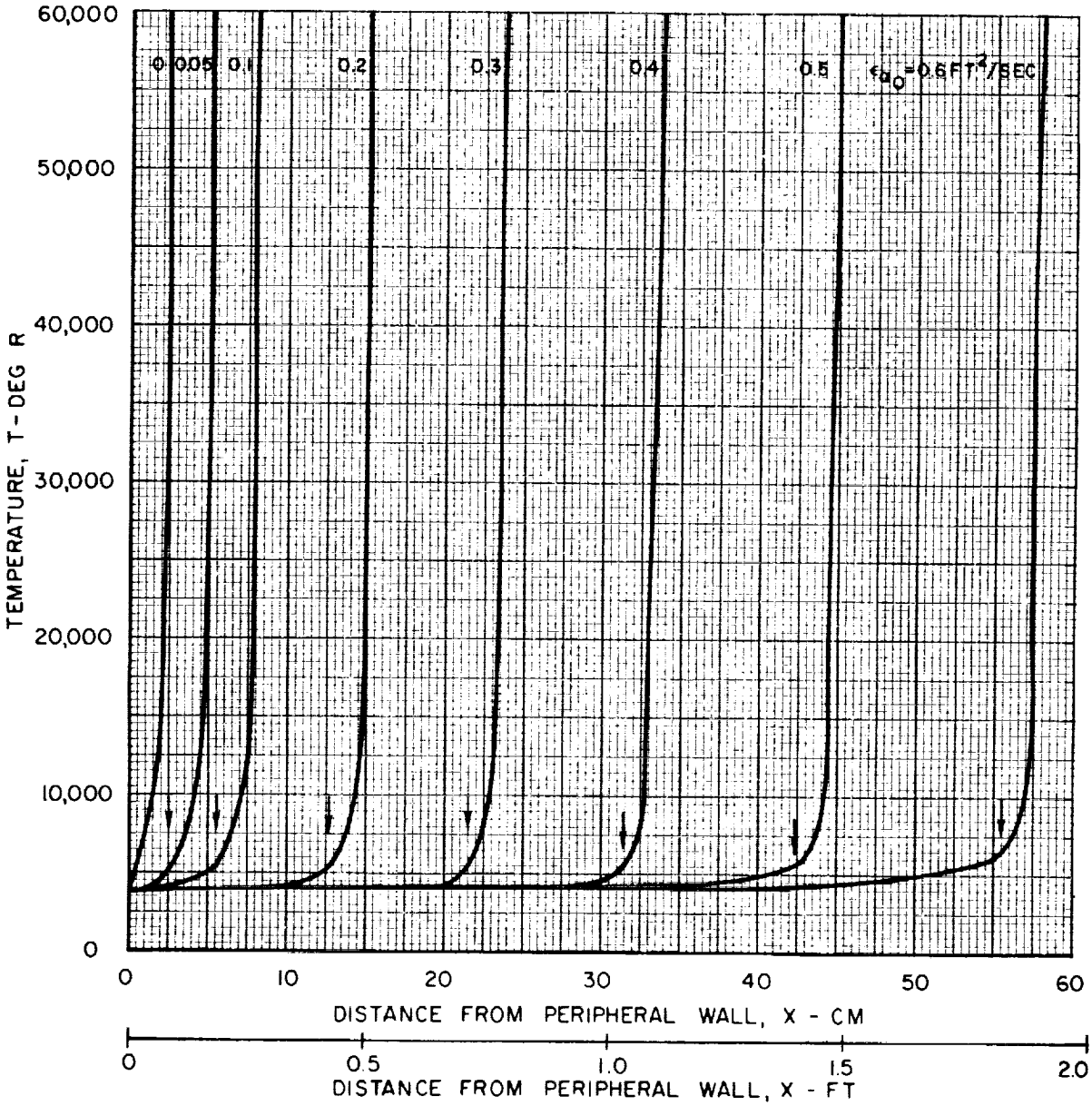

FIG. 26

EFFECT OF EXPONENT IN CIRCULATION PROFILE LAW AND PERIPHERAL WALL TURBULENT HEAT DIFFUSIVITY ON WIDTH OF TURBULENT ZONE

WIDTH OF TURBULENT ZONE DEFINED AS DISTANCE FROM PERIPHERAL WALL AT WHICH $Ri \geq 1.0$

$W_R = 1.0\ LB \cdot SEC^{-1} \cdot FT^2$

$r_1 = 100\ CM$

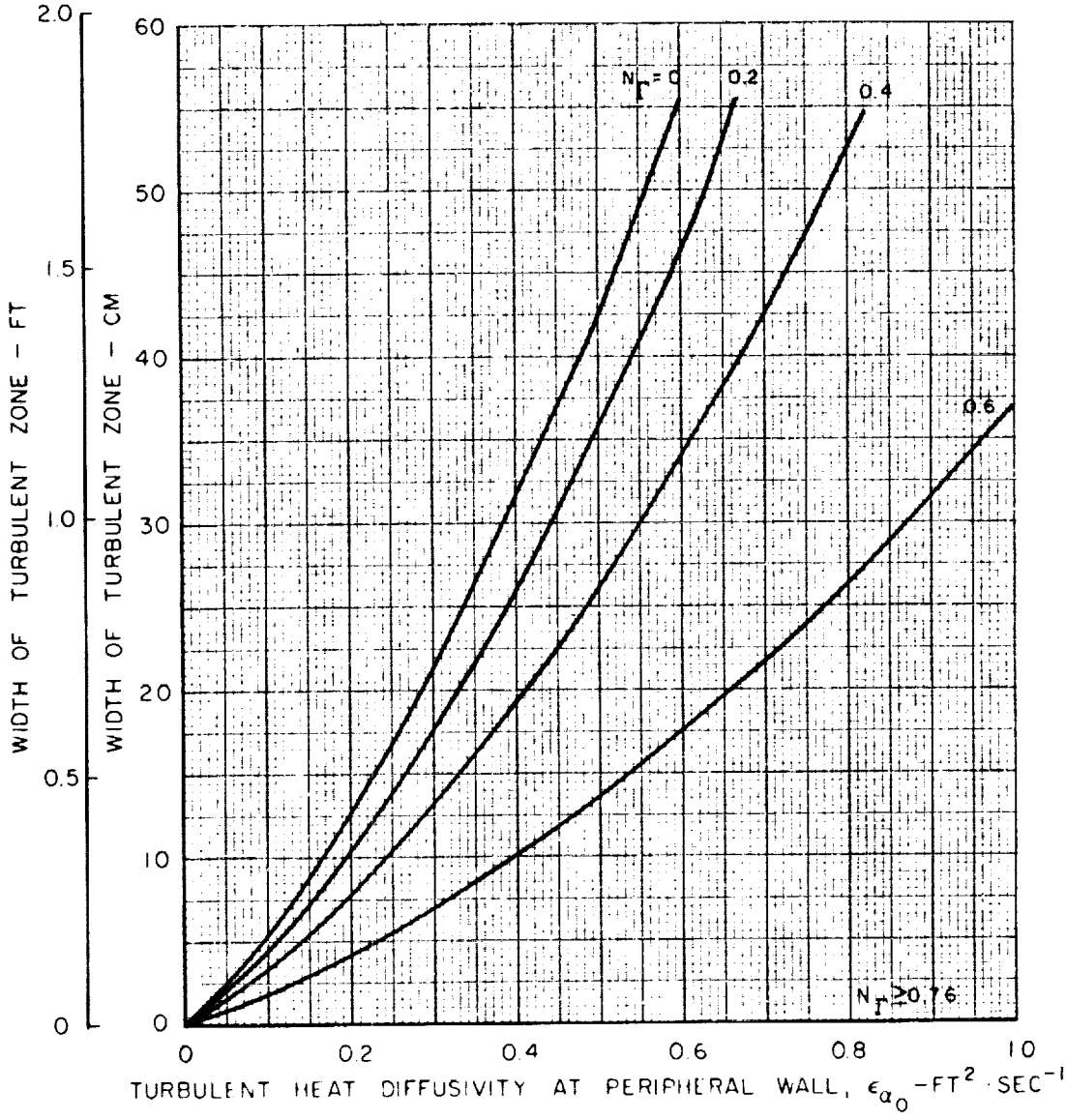

NASA-Langley, 1967 CR-694